INVESTIGATION OF SEISMIC DATA AMPLIFICATION RESPONSE UNDER THE SAND DUNES OF RUB AL-KHALI

BY

MUSTAFA AHMED AL-MARZOOQ

A Thesis Presented to the

DEANSHIP OF GRADUATE STUDIES

KING FAHD UNIVERSITY OF PETROLEUM & MINERALS

DHAHRAN, SAUDI ARABIA

In Partial Fulfillment of the

Requirements for the Degree of

MASTER OF SCIENCE

In

GEOPHYSICS

May 2017

KING FAHD UNIVERSITY OF PETROLEUM & MINERALS

DHAHRAN- 31261, SAUDI ARABIA

DEANSHIP OF GRADUATE STUDIES

This thesis, written by Mustafa Ahmed Al-Marzooq under the direction his thesis advisor and approved by his thesis committee, has been presented and accepted by the Dean of Graduate Studies, in partial fulfillment of the requirements for the degree of **MASTER OF SCIENCE IN GEOPHYSICS.**

Dr. Abdulaziz Al-Shaibani
Department Chairman

Dr. SanLinn Isma'il Kaka
(Advisor)

Dr. Salam A. Zummo
Dean of Graduate Studies

Dr. Abdullatif Al-Shuhail
(Member)

20/12/17

Date

Dr. Mamadou Diallo
(Member)

Dedication

To my lovely parents, caring wife and thoughtful siblings for their prayers, support and patience.

ACKNOWLEDGMENTS

I would like to thank my supervisor Dr. Kaka for the useful comments, remarks, and encouragement throughout the entire process of researching and writing this master thesis. His door was always open whenever I had an issue with my analysis. He directed me in the right the direction whenever he believed I required it. Words can't express how valuable his guidance has been. I am forever grateful to him.

Furthermore, I would like to thank Dr. Diallo for introducing me to the topic as well for his full support during the entire process. Dr. Diallo was involved in the validation of the proposed methodology and synthetics Data. Without his passionate cooperation and input, the validation of the proposed methodology could not have been successfully conducted.

I would like to thank Dr. Abdullatif Al-Shuhail for his remarks, and for sharing his precious time willingly during the process of research. I am gratefully indebted to him for his valuable comments.

I wish to express my sincere gratitude my loving parents, caring siblings, lovely fiancée and my loved ones, who have supported me throughout my entire master study, by keeping me optimistic. I will be thankful forever for your love.

A very special gratitude goes out to all down at Saudi Aramco for helping and providing the data for the study.

I also put on record my sincere appreciation to all, who directly or indirectly, have lent their hand in this research.

TABLE OF CONTENTS

.

ACKNOWLEDGMENTS ..... **V**

TABLE OF CONTENTS ..... **VI**

LIST OF TABLES ..... **VIII**

LIST OF FIGURES ..... **IX**

LIST OF ABBREVIATIONS ..... **XIII**

ABSTRACT ..... **XIV**

ملخص الرسالة ..... **XV**

CHAPTER 1 INTRODUCTION **1**

1.1 Thesis outline **3**

1.2 Data quality in Rub Al-Khali **4**

1.3 Study Site **6**

1.4 Objectives **8**

CHAPTER 2 LITERATURE REVIEW **9**

2.1 The amplification factors **10**

2.1.1 Impedance contrast **11**

2.1.2 Resonance effects **13**

2.1.3 Surface wave generation and Scattering **15**

2.2 Attenuation **16**

2.3 Amplitude correction methods **17**

2.4 Numerical Simulation 20
2.5 Spectral Analysis of Signals 21
CHAPTER 3 METHODOLOGY 23
CHAPTER 4 NUMERICAL SIMULATION 27
4.1 Model parameter 27
4.2 Model Design 28
4.3 Results 30
CHAPTER 5 REAL DATA ANALYSIS 34
5.1 Acquisition parameter for the 2D real data set 34
5.2 Operator design window 35
5.3 Amplification as a function of soil thickness 37
5.4 Amplification as function of offset 40
5.5 Resonance frequency 41
CHAPTER 6 METHODOLOGY APPLICATION 45
CHAPTER 7 CONCLUSIONS AND RECOMMENDATIONS 64
7.1 Conclusions 64
7.2 Limitation and Recommendation 65
BIBLIOGRAPHY 67
VITAE 72

LIST OF TABLES

Table 4.1 Modeling parameter 29

LIST OF FIGURES

Figure 1.1 The influence of different emission conditions on the recorded signal. a) Shooting at the Sabkha results in weak noise and high signal to noise ratio (S/N). b) Shooting at the top of the sand dune results in high noise and low S/N. The red and blue curves represent the elevation in meters and the short wavelength statics values in milliseconds, respectively. 5
Figure 1.2 The amplitude spectra of 20 traces with the same offset (700 m). The curves are colored by the receiver statics values as indicated in the legend. Note that the highest amplification occurs on the low frequency bandwidth..... 6
Figure 1.3 The Rub' Al-Khali desert in Saudi Arabia,: one of the world's largest deserts, The Rub Al-Khali has dunes separated by highly reflective Sabkha crust, formaing the unusual blueish color observed in the satellite images..... 7
Figure 3.1. The average amplitude spectra associated with several stations for synthetic (a) and real data sets (b). The entire trace was used to compute the average amplitude spectra of the traces corresponding to each station. The black curves represent the average amplitude spectra for stations positioned in the Sabkha, while the red and blue curves represent the average amplitude spectra of sand dune stations before and after application of the amplitude correction respectively. 26
Figure 4.1 The wavelet shape in time domain (a) and the corresponding frequency amplitude and phase spectrum (b) 28
Figure 4.2 S-wave (a) and P-wave (b) 2D velocity model consisting of a four-layer model (air, Sabkha, two clastic layers), with an eclipse-shaped hill layer that represents sand dunes..... 29
Figure 4.3 The result of running the simulation source placed at 1 m. The red curves on the top represent the corresponding RMS amplitude..... 31
Figure 4.4 The same record as Figure 4.3 after sand dune amplification correction. The blue and red curves on the top represent the corresponding RMS amplitude before and after application of the amplitude correction, respectively. A threshold of .000015 was placed on the RMS computation of the near offset traces. 32
Figure 4.5 The average amplitude spectra associated with several stations for synthetic (a) and real data sets (b). The entire trace was used to compute the average amplitude spectra of the traces corresponding to each station. The black curves represent the average amplitude spectra for stations positioned in the Sabkha, while the red and blue curves represent the average amplitude spectra of sand dune stations before and after application of the amplitude correction respectively. 33

Figure 5.1 histogram of offset distributions within a seismic survey. (a) All the traces, (B) and (C) the Sabkha and dune traces respectively 35
Figure 5.2 The GRT spectra using different range of offsets. The graph is displayed with frequency- x-axis, in Hertz, and a log-amplitude y-axis..... 36
Figure 5.3 The effects of choosing a different offset range for computation of the sand dune amplification correction for the shot gather. The green curve on the top represents the sand dune elevation, and the red and blue curves represent the RMS amplitude before and after the application of the sand dune amplification correction respectively..... 37
Figure 5.4 The average amplitude spectrum for the sand dunes stations verse the corresponding statics corrections with the fitted linear regression line..... 39
Figure 5.5 The regression lines associated with different series of 10-Hz-wide window for averaging the amplitude spectrum and the corresponding statics corrections..... 40
Figure 5.6 Comparison between the average amplitude spectrum between the Sabkha traces and the sand dune traces at different offset ranges..... 41
Figure 5.7 Sand Curve (Robinson & Al-Husseini, 1982) gives the transit time of P-waves in sand and the thickness of dunes. 42
Figure 5.8 Resonance curve: gives the soil natural frequency of the sand and the thickness of dunes..... 43
Figure 5.9 A comparison between the theoretical and observed resonant frequency. (a) The Elevation profile (b) The computed and observed (c) resonant frequency..... 44
Figure 5.10 A comparison between the theoretical and observed resonant frequency. (a) The Elevation profile (b) The computed and observed (c) resonant frequency..... 44
Figure 6.1 Representative shot gathers. a) A raw field record with geometric spreading correction applied. b) The same record as Figure 5a after the application of statics correction. The red curve at the top represents the elevation. 46
Figure 6.2 A raw field record with spherical divergance correction (far left panel) and its bandpass-filtered versions. The blue and red curves on the top represent sand dune elevation and the RMS amplitude, respectively. Note the amplification and a low S/N in the traces collected in the sand dunes..... 48
Figure 6.3 The same field record as in Figure 6.2 and its bandpass-filtered versions following application of the sand dune amplification correction. The blue and red curves on the top represent the sand dune elevation and the RMS amplitude, respectively. 49
Figure 6.4 The corresponding F-K spectra for data shown in Figure 9a and Figure 10a on a decibel scale. The graph is displayed with frequency- y-axis, in

Hertz, and wavenumber x-axis, in 1/m, the colors represent the relative energy in decibel 49
Figure 6.5 The average amplitude spectra associated with several stations. The entire trace was used to compute the average amplitude spectra of the traces corresponding to each station. The black curves represent the average amplitude spectra for stations positioned in the Sabkha, while the red and blue curves represent the average amplitude spectra of sand dune stations before and after application of the amplitude correction respectively. 50
Figure 6.6. Near offset gather for a) only geometric spreading correction, and b) the same record as Figure 11a after sand dune amplification correction. The green curve on the top represents the elevation of the sand dune, and the red and blue curves represent the RMS amplitude before and after the application of the sand dune amplification correction respectively. 51
Figure 6.7. Mid offset gather for a) only geometric spreading correction, and b) the same record as Figure 1a after sand dune amplification correction. The green curve on the top represents the sand-dune elevation, and the red and blue curves represent the RMS amplitude before and after the application of the sand dune amplification correction respectively. 52
Figure 6.8. Far offset gather for a) only geometric spreading correction, and b) the same record as Figure 13a after sand dune amplification correction. The green curve on the top represents the sand dune elevation, and the red and blue curves represent the RMS amplitude before and after the application of the sand dune amplification correction respectively. 53
Figure 6.9 CMP offset gather with spherical divergence, NMO and Mute applied (a) and (b) shows the same record as Figure 6.9a after sand dune amplification correction. The green curve on the top represents the short wavelength statics in ms, the red and blue curves represent the RMS amplitude before and after the application amplification correction respectively. 54
Figure 6.10 A portion of a CMP stack before and after the application of sand-dune amplification correction. The green curve the green curve on the top represents the elevation of the sand dune, and the red and blue curves represent the RMS amplitude before and after the application amplification correction respectively. 55
Figure 6.11 The average amplitude spectrum associated with the first 100 station. The graph is displayed with frequency- y-axis, in Hertz, and station number x-axis, the z-axis represent the relative amplitude energy in decibel 56
Figure 6.12 The average amplitude spectrum associated with the first 100 station. The graph is displayed with frequency- y-axis, in Hertz, and station number x-axis, the z-axis represent the relative amplitude energy in decibel 57
Figure 6.13 Procesing flow applied to the real data set 58

Figure 6.14 A raw field record with geometric spreading correction. The blue and red curves on the top represent sand dune elevation and the RMS amplitude, respectively. 60
Figure 6.15 The same field record as in Figure 6.14 following the application of the sand dune amplification correction. The blue and red curves on the top represent the sand dune elevation and the RMS amplitude, respectively. 61
Figure 6.16 A portion of a CMP final stack before migration without the application of the sand dune amplification correction. 62
Figure 6.17 A portion of a CMP final stack before migration with the application of the sand dune amplification correction. 63

LIST OF ABBREVIATIONS

AVO	Amplitude Variation with Offset
FDM	Finite Difference Method
FEM	Finite Element Method
GRT	Global Reference Trace
LRT	Local Reference Trace
PML	Perfectly Matched Layer
RMS	Root Mean Squire
SSG	Standard Staggered-grid

ABSTRACT

Full Name : Mustafa Al-Marzooq

Thesis Title : INVESTIGATION OF SEISMIC DATA AMPLIFICATION RESPONSE UNDER THE SAND DUNES OF RUB AL-KHALI

Major Field : Geophysics

Date of Degree : 10/2017

The Rub Al-Khali region in Saudi Arabia is characterized by the presence of sand dunes separated by salt flats (Sabkhas). In general, dunes' elevations vary between 90 m and 250 m. The presence of these sand dunes along with the rapidly varying surface topography pose logistical challenges for seismic data acquisition and processing, especially when the objective is to produce processed data that are suitable for amplitude versus offset (AVO) analysis. Indeed, the high contrast in acoustic impedance between the dune base and the underlying formation results in an amplification of seismic waves recorded at stations located on the surface. Furthermore, reverberations (resonance) of seismic waves within the sand dunes and scattering around topographic irregularities may sometime strengthen the effects of the amplification. These amplification effects need to be mitigated early in the processing stage, otherwise subsequent attempts to address the issue using conventional surface consistent amplitude correction (SCAC) methods will fail, and thus compromises the suitability of the processed data for AVO analysis. In this study, I propose a new method to reduce the effects of sand dune amplification in a surface-consistent manner. The proposed method is examined using real data from the Rub Al-Khali region. In addition, the effects of the new SCAC method on subsequence processes is examined with the purpose of obtaining wideband seismic data to benefit AVO analyses. Finally, the study also investigates the sand dune effects and assesses the performance of the proposed method by running an optimized finite-difference modelling scheme. The method developed in this study significantly reduces sand dune amplification effects in a surface consistent manner, and thus provides a dataset that may be suitable for further AVO analyses.

ملخص الرسالة

الاسم الكامل:مصطفى أحمد ماجد آل مرزوق

عنوان الرسالة: التحقيق من تضخم السعة في البيانات الزلزالية تحت كثبان الربع الخالي

التخصص: جيزفيزياء

تاريخ الدرجة العلمية:

تتميز منطقة الربع الخالي في المملكة العربية السعودية بوجود الكثبان الرملية التي تفصلها الترسبات الملحية (سبخات) والتي يتراوح ارتفاع الكثبان الرميلية فيها بشكل عام بين ٩٠ متر الى ٢٥٠ متر. يشكل وجود هذه الكثبان الرملية جنبا إلى جنب مع تضاريس سطح الأرض المتغيرة تحديات لوجستية من أجل الحصول على البيانات الزلزالية ومعالجتها، لا سيما عندما يكون الهدف هو إنتاج بيانات مناسبة لتحليل السعة مقابل الإزاحة (AVO). في الواقع، إن التباين العالي في المقاومة الصوتية بين قاعدة الكثبان الرملية والسبخات ينتج عنه تضخم لسعة الموجات الزلزالية المسجلة في المحطات الموجودة على سطح الأرض. بالإضافة إلى ذلك فإن صدى الموجات الزلزالية داخل الكثبان الرملية، وتشتتها حول التضاريس الغير المنتظمة قد يعزز من التضخم. هذا التضخم يؤدي إلى فشل الأساليب التقليدية لتصحيح قياس السعة (SCAC)، مما يضر من ملائمة البيانات المعالجة لتحليل AVO. لذا ينبغي تخفيف التضخم في مرحلة مبكرة من مراحل المعالجة. في هذه الدراسة أقترح طريقة جديدة للحد من تضخم السعة نتيجة لوجود الكثبان الرملية بطريقة تلائم التغيرات السطحية. يتم إختبار الطريقة المقترحة باستخدام بيانات حقيقية من منطقة الربع الخالي، بالإضافة إلى ذلك تعرض الدراسة أثر الأسلوب المقترح على عمليات المعالجة اللاحقة بهدف الحصول على بيانات زلزالية عريضة النطاق للاستفادة من تحليلات AVO. أخيرا، تقوم الدراسة بالتحقق من آثار الكثبان الرملية وتقييم آداء الطريقة المقترحة من خلال تقنية نمذجة الفروقات المنتهية. الطريقة التي تم تطويرها في هذه الدراسة تقلل بشكل كبير من آثار التضخم الحاصل لوجود الكثبان الرملية بطريقة ملائمة مع التغييرات السطحية . بالتالي توفر مجموعة بيانات قد تكون مناسبة لمزيد من تحليلات AVO.

CHAPTER 1

INTRODUCTION

In the past, structural mapping has been the main application of seismic reflection profiling in the oil and gas industry. Seismic interpretation has been essentially structural; therefore, little emphasis was put on preserving the amplitude variation during processing. However, with the introduction of bright spot technology and the advances in seismic acquisition and processing, the development of a better true amplitude processing flow has been the subject of much of the geophysical research. Historically, research on bright spot was published in the 1960s but was largely unavailable as most companies developed their AVO methods in secrecy. By 1984, Ostander's research on AVO interpretation techniques led to the confirmation of bright spots. Since then, several groups worldwide have implemented the AVO interpretation techniques to extract more information from seismic amplitude in both pre-stack gathers and stacked seismic sections (Chopra & Castagna, 2014).

However, the reliability of this technique appears to be limited by the assumptions and approximations made in data acquisition and processing flow. These factors include source strength and consistency, array effects, near surface variations, attenuation, dispersion, effect of overburden, phase change with depth and offset, multiples interfering with primaries, ground roll, spherical divergence, and absorption (Downton, Russell, & Lines, 2000). For these reasons, processing seismic data to produce deliverables that are suitable

for AVO analysis requires a carefully designed workflow that preserves the relative amplitude of reflection events as they bounce back from reflecting interfaces. Given the specific nature of the surface topography in the Rub Al-Khali, designing a processing workflow for seismic data acquired in such an environment may be challenging.

The Rub Al-Khali is characterized by sand dunes separated by salt flats, or Sabkhas, which have significant adverse effects on the amplitude variation of seismic reflection events from the target horizon. In addition, the high impedance contrast between sand dunes and underlying formations introduces a frequency-dependent amplification (Friedmann, 1988). This significantly alters the relative signal amplitudes recorded from dune and Sabkha locations, thus compromising the preservation of the actual AVO trend from reflection boundaries. Furthermore, reverberations (resonance) of seismic waves within sand dunes and scattering around topographic irregularities may sometimes strengthen the effects of the amplification. Other factors include the following: topographic scattering, P-to-S mode conversion, elastic attenuation, and surface wave generation.

Published surface-consistent amplitude correction methods use optimization schemes to estimate a correction factor for each component in the spectral decomposition equation (Cambois & Stoffa, 1992; Cary & Lorentz, 1992; Levin, 1989; Taner & Koehler, 1981). However, application of these methods to datasets acquired in the Rub Al-Khali were insufficient to fully correct for the spurious amplification effects of sand dunes. As a result, exploring new ways or alternative remediation to the amplification effects of sand dunes is necessary, and is the focus in of this study.

In this study, I describe a new deterministic method to reduce amplification effects caused by the presence of sand dunes in a surface-consistent manner. This method (Saudi Aramco U.S. Patent Application No. 15/229,669) is similar to the standard spectral ratio technique, commonly used in earthquake and engineering studies (Bonilla, Steidl, Lindley, Tumarkin, & Archuleta, 1997; Borcherdt, 1970; Field & Jacob, 1995; Frankel, Carver, & Williams, 2002; Parolai, Bindi, & Augliera, 2000). It uses a deterministic approach to derive surface-consistent, frequency-dependent de-amplification functions.

1.1 Thesis outline

In chapter 2, I review the current practice of dealing with the undesired effects of near-surface features on the amplitudes of seismic reflections. In addition, I examine the causes of seismic amplification in the alluvial environment. In chapter 3, a method that deals with the undesired effect of sand dunes amplification is proposed. The chapter also presents the prerequisites of using this method and where it fit in the processing flow. The 2-D model and the results are discussed in chapter 4. In this chapter, I also review the limitation of the 2D finite difference methods. In chapter 5, I analyze the real data geometry for two field surveys carried out in Rub-Al-Khali, along with some relevant field parameters, such as elevation, maximum offset, and sources and receivers used. In chapter 6, the application of the newly proposed method is tested on the real data set. A case study is also discussed in chapter 6, where field seismic data from one of the surveys is used to generate two stacked sections using two different workflows. Chapter 7 concludes this study with a number of remarks drawn from it. It also suggests future work to improve the correction method discussed.

1.2 Data quality in Rub Al-Khali

Figure 1.1 shows the amplification effects of sand dunes on two shot gathers from a 2D seismic survey carried out in Rub Al-Khali. The two shots are 120 m apart, and share a half spread. The data was acquired with 10m receiver station intervals and 5m source station intervals with five vibroseis sweeps per source station. The source location was placed at the middle of the receiver array with 600 channels at both ends. The Sabkha floor was located at an elevation of 75 m above mean sea level, and was slightly inclined toward the west. The elevation profile and receivers' sand dunes statics (not-applied) were plotted above the gathers to illustrate the magnitude of these corrections, which were consistent with the elevation of the sand dunes as expected. The first record of Figure 1.1a, where the source is located in the Sabkha, illustrates clear demarcation in amplitude variation, coinciding with the sand dune location. The record was contaminated by coherent and high amplitude back-scattered waves associated with the rough topography of the dunes, which obscured reflectors from deeper layers. No clear reflection could be identified under the dunes. Figure 1.1b illustrates a case where the shot is placed on the sand dunes. The seismic record was contaminated by high amplitude caused by high contrast in acoustic impedance between the Sabkha and sand dunes, and the reverberation of waves trapped within the sand dune layer. The amplification that occurred when the receivers were positioned in the sand dunes was mostly due to the seismic waves propagating from a medium with high acoustic impedance (salt flat) into a medium with very low acoustic impedance (dune consists of non-cohesive loose sand grains). In contrast, the seismic waves emanating from

source points on elevated sand dunes propagated from a medium with low acoustic impedance (sand dune) into a medium with high acoustic impedance (salt flat). Consequently, seismic waves transmitted through the base of sand experience reduced the amplitude. Nevertheless, I found that traces with a source and receiver positioned in the same sand dune showed strong reverberations and amplification effects due to the high reflectivity contrast between the sand dunes and the Sabkha. These observations are consistent with the underlying physics of seismic energy partition at interfaces.

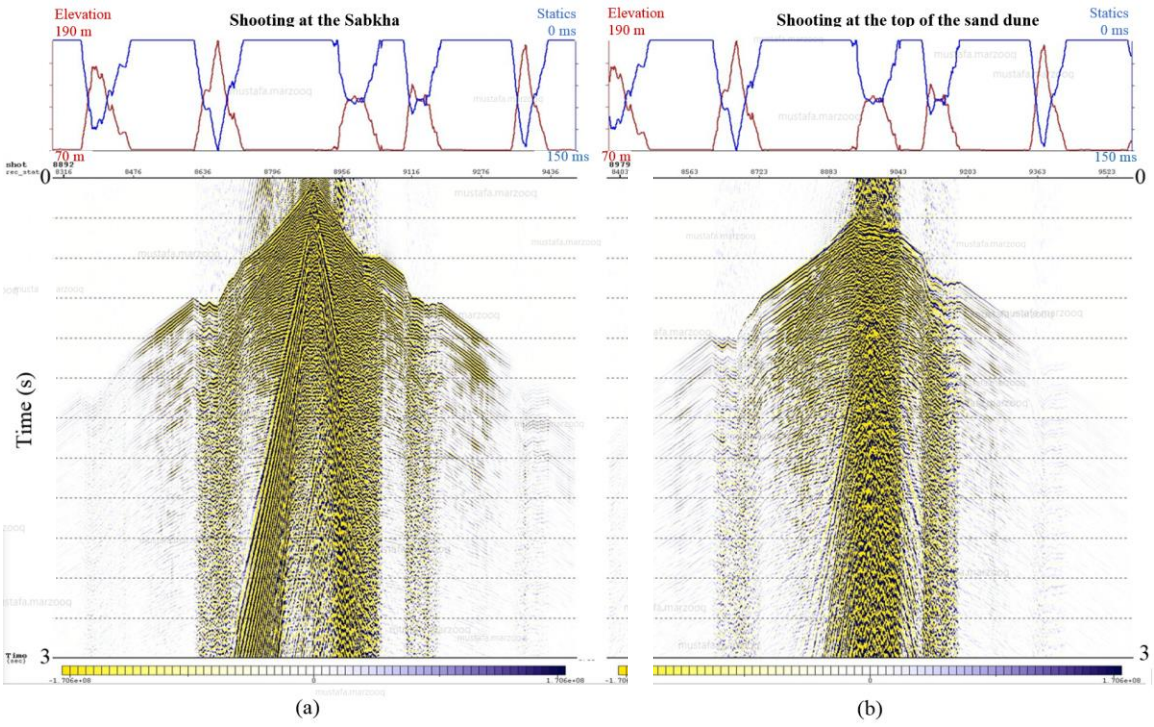

Figure 1.1 The influence of different emission conditions on the recorded seismic signal. a) Shooting at the Sabkha results in weak noise and high signal-to-noise ratio (S/N). b) Shooting at the top of the sand dune results in high noise and low S/N. The red and blue curves represent the elevation in meters and the short wavelength statics values in milliseconds, respectively.

Figure 1.2 shows the amplitude spectra of 20 traces with the same offset (700 m), color-coded from yellow to black, based on the extent of static correction (yellow: no sand

dune static correction; black: largest sand dune static correction), confirming that the sand dunes were responsible for the observed amplification. Note that the highest amplification occurs at 20 Hz.

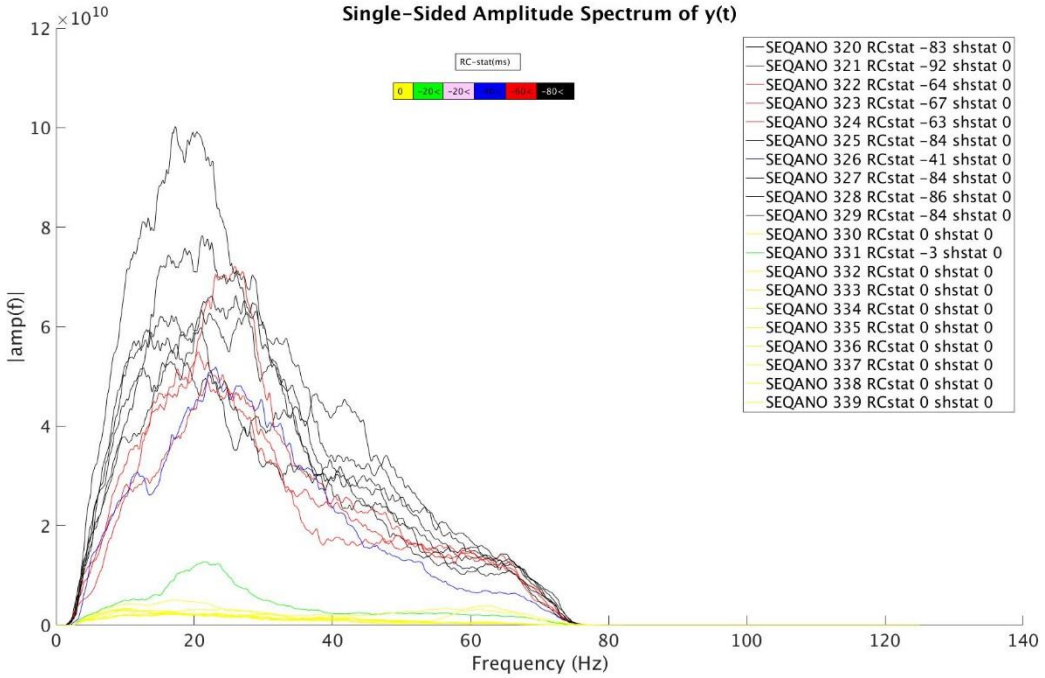

Figure 1.2 The amplitude spectra of 20 traces with the same offset (700 m). The curves are colored by the receiver statics values as indicated in the legend. Note that the highest amplification occurs on the low frequency bandwidth.

1.3 Study Site

Rub Al-Khali is a vast desert covering over 250,000 square miles of the Southern Arabian Peninsula (Figure 1.3). The structural basin within this region occupies a substantial portion of Saudi Arabia, with an estimated length of 1,000 kilometers and width of 500 kilometers. The average elevation of sand dunes is generally 91 meters, and, at times, they reach in excess of 183 meter (Robinson & Al-Husseini,

1982). Moreover, the dunes, which sit on a flat Sabkha base, are covered by pink and white alternating bands of sand, which creates a rippling pattern. In 1982, Robinson and Al-Husseini (1982) developed an empirical relationship between the transit time of P-waves in sand and the elevation of dunes. They used that relationship, commonly known as the sand curve method, to derive sand dune statics for seismic data from the Rub Al-Khali region. Seismic data collected in Rub al-Khali has always been poor, low signal-to-noise ratio (S/N), and this study attempts to consider developing a new method to improve it.

Figure 1.3 The Rub' Al-Khali desert in Saudi Arabia,: one of the world's largest deserts, The Rub Al-Khali has dunes separated by highly reflective Sabkha crust, forming the unusual blueish color in the satellite pictures.

1.4 Objectives

The primary objective of this study is to develop a new method that significantly reduce the sand dune amplification effects using real data from the Rub Al-Khali region. In addition, a workflow to improve the signal to noise ratio from Rub Al-Khali is examined. To achieve these objectives, two approaches were taken. First, 2-D model representatives of the sand dune/Sabkha environment were used to generate synthetic seismic gathers to assess the performance of the proposed method. Second, two different processing workflows were implemented to the same seismic dataset to assess the effect of the new amplitude correction method on the final stack.

CHAPTER 2

LITERATURE REVIEW

The present literature review includes contributions from a variety of disciplines. A significant amount of research on site amplification factors has been published in the Earthquake Engineering literature. Additionally, the methodology used in this study is similar to the standard spectral ratio technique, which is commonly used in the earthquake and engineering studies (Borcherdt, 1970; Bonilla et al. 1997; Field & Jacob, 1995; Parolai et al. 2000). The methodology also feeds from a great amount of work done in surface consistent correction methods (Taner & Koehler, 1981; Levin, 1989; Cambois & Stoffa, 1992; Cary & Lorentz, 1992). Furthermore, the presentation of the finite difference modeling technique and implementation come from computational physics studies. A comprehensive review of all these areas is beyond the scope of this thesis. Attempts to cover such a variety of topics in a comprehensive manner would undoubtedly fail to adequately cover all the important research performed in each of these individual areas of study. In this chapter, only a brief synopsis of the amplification factors and the treatment of sand dune effects by current conventional workflow is presented. The aim is to provide the reader with a general knowledge of the foundations upon which this work is grounded.

2.1 The amplification factors

It is well known that local site conditions can modify the main characteristics of the seismic waves (amplitude, frequency contents, and duration), in comparison to the surrounding rock (Anderson et al. 1986; Bard & Bouchon 1980; Bonilla et al. 1997). Holzer (1994), for example, noted that the intensity of ground shaking was irregular all over the city of Los Angeles even within short distances (1 Km). The same inconsistency in response was also noted in the exploration surveys conducted in desert environment. Friedmann (1988) noted that the sand dunes respond much differently than the hard Sabkha layer to the seismic excitation, and thus alter the relative amplitudes of signal recorded on dune and Sabkha locations. This discrepancy in seismic response implies that the effects of site conditions are major factors to be considered (Adan & Rollins, 1993; Holzer, 1994). It is, therefore, important to understand the causes of seismic amplification, to mitigate the variation within the processing workflow. Several factors have been associated with data amplification in seismic wave studies in areas with different thickness of sand dunes. These factors include the following: Impedance contrast, resonance effects, P-to-S wave conversation, damping, sand dune thickness, surface wave generation, and scattering.

Olsen and Schuster (1995) used the finite difference modeling schemes to identify the major causes of seismic amplification in the Salt Lake Basin. They showed that several factors contribute to the observed amplification in the low-frequency band in the semi-consolidated deposits of the Salt Lake Basin— reverberation within the shallow deposits,

the high impedance contrast between basin sediments and the higher velocity underlying bedrock, P to S mode conversion, surface-wave generation, and reverberation.

2.1.1 Impedance contrast

When the earth is excited by a vibrosieis or a fault ruptures, waves travel away from the source in all direction. Since the earth is composed of a complex mixture of rocks and sediments of several types, as the waves reach boundaries between different rock types, they are reflected and refracted. Near the surficial layer, where the density and propagation velocity are generally lower than the bed rock below it, the reflected ray that strikes the horizontal boundaries changes its propagation direction to a nearly vertical direction. The fundamental mechanism responsible for the amplification in sand dunes is the trapping of seismic waves, attributed to the high impedance contrast between sediments and the underlying formation. The impedance contrast is defined as the ratio between the wave velocity and density of different geologic materials (Bard & Bouchon, 1980; Kawase & Aki, 1989).

Seismic waves travel slower through soft loose sediments than through dense stiff sediments. The wave slows down as it travels from harder to softer rock,, and therefore the conservation of energy entails that the amplitude must increase as the energy flux must remain constant. Quantitatively, for a very simple horizontal 1D site, the energy is given by Karmer (1960).

$$E = p * V * u \qquad (2.1)$$

Where E is the energy per unit volume, p is the density, V and u are the velocity and particle velocity respectively. As the wave reflects back to the surface through the loose near surface layer, the density and shear wave velocity decrease; consequently, the particle velocity ů must increase to compensate the decrease in density and velocity. Both impedance (resistance to particle motion) and damping (attenuation) affect the amplitude of ground motion. For the simple case of normal incident, the transmission coefficient (T) equation is used to obtain an approximate of the impedance effects at the sand dune-Sabkha interface.

$$T = \frac{2Z_1}{Z_1+Z_2} = \frac{2\rho_1 V_1}{\rho_1 V_1+\rho_2 V_2} \qquad (2.2)$$

The subscripts 1 and 2 denote the incident and transmitting medium, while ρ and V represent the density and velocity of the medium with Z representing the acoustic impedance. From this equation, one can see that if the acoustic impedance of the incident medium is larger than the transmitting medium (i.e., $\rho_1 V_1 > \rho_2 V_2$), the transmission coefficient will be greater than one. The transmission coefficient for typical velocity and density values for a sand dune (400–1200 m/s and 1.7–1.9 g/cm3) and Sabkha (2000–3000 m/s and 2.1–2.3 g/cm3) ranges between 1.5 and1.8. For that reason, the variation in response between the sand dune and Sabkha must be attenuated prior to application of surface-consistent scaling methods.

Two-dimensional seismic ground response studies have been carried out by Benz and Smith (1988) to identify the major causes of the observed low frequency amplification in the Salt Lake Basin. The simulation results were compared with the observed amplitude values in the Salt Lake Basin that show a ten times higher amplification within the valley

than measured values on reference rock sites. The synthetic seismograms suggested that the high impedance contrast contribute to at least one-half of the site low-frequency amplification. Joyner (1992) studied the peak horizontal accelerations and peak horizontal velocity records from the 1979 Imperial Valley earthquake of California. The simulation response for a layered viscoelastic model and the field data showed fair agreement in the spectrum shape. The result shows that the observed site amplification may be more of the simple effect of the low near-surface velocity, and less of a matter of reverberation of seismic waves. Furthermore, the agreement between the observed resonant frequency and the computed fundamental frequency suggest that there is no indication of nonlinear sediments response. Shibuya (1992) analyzed the numerical results from typical sedimentary basin shapes and showed that amplitudes of local surface-waves are dependent on the high impedance contrast between basin sediments and the higher velocity underlying bedrock.

2.1.2 Resonance effects

The degree of the amplification is also affected by the reverberations (resonance) of seismic waves within the soft sedimentary cover at the soil natural frequency. For a layer with a rigid interface at the bottom and a free-surface at the top, the horizontal displacement is given by (Cantore, 2008).

$$u(z,t) = Ae^{i(\omega t - kz)} + Be^{i(\omega t + kz)} \qquad (2.3)$$

Where ω is the circular frequency, k is the wavenumber (ω/Vs), A and B represent the amplitude of the waves traveling in the +z direction and –z direction, respectively. From

the equation, note that the shear stress, and consequently the shear strain, vanish at the free surface (z=0), that is:

$$\tau(0,t) = G\gamma(0,t) = G\frac{\delta u(0,t)}{\delta z} = 0 \qquad (2.4)$$

. Substituting Equation 2.3 in 2.4 and differentiate yield:

The displacement of the constructive interference of two waves produce a fixed shape standing wave with respect to depth and can be expressed by the following:

$$u(z,t) = 2Ae^{i(\omega t)}\frac{e^{i(kz)}+e^{-i(kz)}}{2} = 2A\cos(kz)\,e^{i(\omega t)} \quad (2.4)$$

The equation can be used to derive a transfer function to describe how each frequency in the bedrock motion is altered by the sand layer between the top and bottom of the soil layer; the transfer function ($F(\omega)$) is given by the following: (Kostadinov & Towhata,2002)

$$F(\omega) = \frac{2Ae^{i(\omega t)}}{2A\cos(kH)e^{i(wt)}} = \frac{1}{\cos(\frac{\omega H}{V_s})} \quad (2.5)$$

Where H represents the thickness of the soil layer. The transfer function indicates that the surface displacement is much larger at certain frequencies than and at least as large as the bedrock displacement (since the denominator can never be greater than 1). As ωH/V approaches $\pi(\frac{1}{2}+n)$, the denominator of equation (1.7) approaches zero, which causes infinite amplification. This simple homogeneous model illustrates that the response of soft soil is strongly dependent upon the frequency of the motion, and the frequencies at which great amplification occurs are related to wave velocities (p and S wave) and the thickness

of the soil layer. At frequencies that approach the fundamental frequency of a soil deposit, the transfer function takes large values. For one-layer 1D structures, the fundamental frequency is given by Olsen & Schuster (1995) as follows:

$$f^p = \frac{V_p}{4H} \quad (2.6)$$

$$f^s = \frac{V_s}{4H} \quad (2.7)$$

Where V_p and V_s are the P-wave and S-wave velocities of the sand dune layer. From the equation, note that the maximum mean vertical-component ratios at low frequencies overlie the thickest sand dunes.

Moczo et al. (1992) investigated 2D resonance phenomena within several classes of the sedimentary structures using the finite-difference modeling. The synthetic seismogram results showed that the resonance phenomenon contributes to the observed amplification and that it is to be expected in any sediment basin. Pratt et al. (2002) using finite difference schemes modeled the U.S. Pacific Northwest sedimentary basin. The simulation result showed that most of the observed amplification could be caused by resonance effects in the low-impedance sediments constituting the upper 550 m of the Pacific Northwest basin. Also, the simulation showed that the generated surface waves contributed significantly to the amplification at the later arrivals. These results indicate the significance of shallow sediments in determining ground motions over thick basins.

2.1.3 Surface wave generation and Scattering

Surface waves generation caused by the rough topography was noted by several authors (Bard & Bouchon 1980; Frankel et al., 1991). The surface waves are generally described by their dispersive velocity and high amplitudes that significantly influence the signal

amplitude. Loukakis and Bielak (1995), based on the 2D and 3D finite difference seismic simulation response of typical sedimentary basin geometry, concluded that surface-wave amplification is strongest when the angle of incidence is at the critical angle, when the horizontal component of the S-wave velocity equals the P-wave velocity and a strong coupling occurs. Xu (1995) 2-D seismic simulation result showed that the signal duration and kinetic energy increased by 15 percent when the seismic scattering was considered. Olsen (1995) found that the scattering effect caused by the neighboring mountains is causing 40 percent of the observed amplification. Rodgers et al. (2010) showed, using three-dimensional simulations, significant mode conversion and scattering around topographic irregularities with amplification of the high frequency band (2 to 8 Hertz) shear waves relative to the flat Earth case.

2.2 Attenuation

Seismic attenuation describes the amplitude loss initiated by the spherical divergence of the seismic waves as they propagate. Attenuation is amongst the primary contributing factors of the site effects. Whilst the impedance contrast between the soil layer and the underlying formation is the dominant factor for the site amplification, attenuation weakens seismic energy and restrains the amplification effects. Attenuation is greatest in soft/loose sediments and partially counters the increase in seismic amplitude from resonance. Furthermore, the amplitudes of lower frequency components attenuate slower than higher frequency components over the same depth (Kjartansson 1979, Dasgupta, & Clark, 1998). Malagnini, L. (1996) showed that while unconsolidated or poorly consolidated sediments may cause significant amplification of seismic ground motion; energy attenuation in sediments can be high as well, thus acting as a counter contributor

to signal amplification. Therefore, a reliable estimate of seismic attenuation, in addition to the site conditions described is critical for the realistic assessment of the seismic hazard in sedimentary deposits. Meng and Dariush (2006) performed a seismic simulation on a soil-rock model with frequency dependent attenuation spectra of soils. The results show that estimating the amplification spectra for the frequency band between 10 and 30 Hz requires a detailed characterization of frequency-dependent attenuation. Estimating the amplification spectra for SH waves propagating through a low impedance soil layer of 100 m thick revealed that a constant assumption of the quality factor (Q) overestimates the amplification spectra at a maximum of seven times at 30 Hz. A frequency-dependent attenuation appears to be significant only at frequencies beyond 10 HZ. Both sediment attenuation and impedance affect the amplitude at the site location.

2.3 Amplitude correction methods

Taner and Koehler (1981) introduced the first surface consistent model used to correct for the undesired effects of near-surface features and the model describes the seismic trace as the convolution of the following four different terms: the source, receiver, common depth point, and offset. Four assumptions were made by Taner and Koehler (1981) to approximate the surface-consistent corrections. They include:

1. All near surface effects are time constant, and they do not vary throughout the recording time.
2. All near surface effects are surface constant, and they do not vary in a spatial manner. This means a receiver related effect will affect all traces recorded from using that receiver in the same manner.

3. The common midpoint assumption (CDP) is valid. This mean a CDP related effect will affect the traces recorded from that CDP gathered in the same manner.
4. The traces must be corrected for normal move out and spherical divergence prior to the application of surface consistent deconvolution methods.

Since their introduction, the surface consistent correction methods (Cambois & Stoffa, 1992, Carey & Gary, 1994; Taner & Kohler 1981; Yu, 1985) became the standard tools to deal with the undesired effects of near-surface features on the amplitudes of seismic reflections from the zone of interest. Nevertheless, application of these methods on dataset from the Rub Al-Khali region has, in general, failed to produce reflection amplitudes that are free from the imprint of these sand dunes.

In conventional surface-consistent amplitude scaling methods, it is typical to try to derive the correction factors from clean seismic data as much as possible by removing any surface consistent noise. This can be difficult when you are dealing with data that is heavily contaminated by noise. As a result, the application of these surface-consistent scaling methods is generally ineffective when applied to dataset from the desert environments that usually exhibit low signal to noise ratio (Robinson & AlHusseini, 1982)

The main shortcoming of the conventional methods is that they yield amplitude scalers for stations (shots/receivers) regardless of whether a station is located on sand dunes or Sabkha. The underlying statistical approach at the core of the conventional methods, prevent this method from the systematic ability to derive scaling factors only for stations impacted by the sand dunes.

In addition, surface consistent scaling methods assume that the noise is Gaussian (Cary & Nagarajappa, 2013); so, large discrepancy on the recorded signal (very high amplitude traces) need to be eliminated from the data being analyzed. In the case of the data from Rub Al-Khali, the unconsolidated sand dunes respond much differently than the harder Sabkha layer to the seismic excitation and often introduce an amplification effect (Friedmann, 1988) on the recorded data. In general, the main reason behind this discrepancy in response is the impedance contrast between the sand dune and Sabkha. The conservation of energy entails that the amplitude must increases as the waves propagate from a stiff rock (with high density and velocity) to a soft rock-with a lower density and velocity. For that reason, this effect has to be eliminated prior to the application of the surface consistent scaling method.

Furthermore, the degree of the amplification is also affected by the reverberations (resonance) of seismic waves within the sand dunes at the soil natural frequency. On the other hand, the amplitude scaling corrections derived using the conventional four-component decomposition (Taner & Koehler, 1981; Vossen, Curtis, Laake, & Trampert, 2006) are frequency independent and, therefore, cannot properly account for the amplification effects associated with sand dunes.

The proposed method uses a deterministic approach to estimate a frequency dependent de-amplification correction for shots and stations located on the dunes only. The method works in a surface consistent manner and is applicable to the entire seismic trace. Only spherical spreading correction and variable gap deconvolution—to attenuate reverberation within sand dunes—may be needed prior to the application of the method.

2.4 Numerical Simulation

There are many methods for simulating wave propagation in a given Earth structure model. The most common methods are as follows: finite element method, finite difference method, pseudospectral and spectral-element methods. In this study, I focus on finite difference method to create the synthetics as it provides a powerful numerical technique for understanding the types of waves that would be produced by a given Earth structure model. Due to its relative precision and computational efficiency, it is the most widely used approach in simulating earthquake movements and it is also turning out to be progressively more vital in the seismic exploration industry.

In general, in the early days, finite difference schemes applied to seismology uses the displacement formulation and conventional one-step Finite Difference (FD) grid; for example, Alterman and Karal (1968), Boore (1970, 1972), Strang and Fix (1973), and Kelly et al. (1976). But the instability and the grid dispersion noted by Levander (1988) in some conventional one-step FD scheme led to the development of staggered grid schemes by Madariaga (1976). The method was further expanded upon by Virieux (1986) and Levander (1988) to include a five coupled elastic equation of velocity and stress relations. The main drawback of these schemes is the high computational cost, and running a numerical modeling on a sequential platform limits the size of the model. To overcome the issue, I use an optimized scheme developed by Etienne et al. (2007) that uses a high order in space and solves the second-order wave equation instead of the first-order formulation.

2.5 Spectral Analysis of Signals

Spectral estimate, a powerful technique of signal analysis, is often used to analyze the distribution as a function frequency. The spectral estimation of a discretely sampled signal is often based on procedures employing the Discrete Fourier Transform (DFT). However, Conventional DFT spectral estimations rely on the assumption that the record repeat to infinity; that is, the process is assumed to be composed of a set of harmonically periodic functions at intervals that correspond to the length of the time record. The basic method for estimating the amplitude spectrum is obtained by computing the Fourier transform X($j2\pi f$) of a sampled time series $x(t)$ of finite length N, followed by multiplying the transformed signal by its complex conjugate $X^*(\ j2\pi f)$ and scaling it by the length N of the finite observation.

$$|X(F)| = X(j2\pi f)\ X^*(\ j2\pi f)/\ N \quad \text{(van Drongelen, 2007) (2.8)}$$

Due to its computational efficiency and relative precision, it is the most widely used approach to obtain a rough first spectral estimate for a large class of signal processes. Despite these advantages there are several inherent performance shortcomings in this approach. The first limitation is the variance of the estimate |X(f)| at each frequency. A second limitation is the spectral leakage of energy across frequencies, creating a bias. Therefore, other methods of analysis are needed to get an accurate spectral representation of the investigated signal. One solution to reduce the spectral leakage is to window the sampled signal using a taper that decreases smoothly to zero or near zero at its ends. There are many commonly used and well-known tapered window functions such as rectangular, hamming and Parzen.

The multi-taper approach (Thomson, 1982) is a new novel method that improves the spectral estimate by addressing both leakage and variance in the estimate. In this approach, a set of different orthogonal tapers are used to reduce the leakage of energy across frequencies bins by providing orthogonal samples of the data. The orthogonal samples are used to create different spectral estimates that can be used to compute an average spectrum with reduced variance.

CHAPTER 3

METHODOLOGY

Assuming the following model in the frequency domain for the trace recorded in the desert environment S^{ij} created by shot number i and recorded by receiver j:

$$S^{ij}(\omega) = s^{i}(\omega) \cdot g^{ij}(\omega) \cdot r^{j}(\omega) \qquad (3.1)$$

Where $r^{j}(\omega)$ the receiver spectra at surface location j is, $s^{i}(\omega)$ is the source spectra at surface position i, and $g^{ij}(\omega)$ is the corresponding medium spectra. I assume that $s^{i}(\omega)$ and $r^{j}(\omega)$ are surface consistent. This means that effects related to a particular source or receiver remain constant for each frequency throughout the whole recording time. I also assume that the source and receiver spectra at the Sabkha is equal to 1. The objective at this stage is to remove the sand dunes effect form the shots. This can be achieved by implementing the following:

1. Compute a global reference trace $U^{gref}(\omega)$ in $(\omega = 2\pi f)$, where f is the temporal frequency needed to determine the sand frequency dependent de-amplification functions. The global reference trace is the average amplitude spectra of all traces from pairs of sources and receivers located on the Sabkha. It is computed for each receiver line and shot line in a 3D survey, and only one is needed in a 2D survey. In the computation of the amplitude spectra, I use the multi taper method (Lees & Parks, 1995) to minimize the spectral leakage and variance in the estimate and derive the global reference as:

$$U^{gref}(\omega) = \sum_{k=1}^{N} \frac{\left|S_k^{ij}(\omega)\right|}{N}, \quad (3.2)$$

Where N is the number of traces with shot and receiver stations located in Sabkha areas within the desired offset range, and $|S_k^{ij}(\omega)|$ represents the amplitude spectrum of a trace with both source and receiver stations in the Sabkha zone.

2. Next, I compute the local reference traces associated with a receiver and shot stations located on a dune elevation. To obtain the optimum result, the computation should cover the same offset range used to derive the global reference trace. However, this might not be achievable in real data due to the survey geometry as well as terrain complexity and access difficulty. For any receiver station J on dune elevation, I compute the corresponding receiver-side local reference trace as the average amplitude spectrum of all M associated seismic traces with shots stations located in the Sabkha.

$$U^{J\_rec}(\omega) = \sum_{k=1}^{M} \frac{|S^{Jk}(\omega)|}{M}. \quad (3.3)$$

3. For any shot station, on dune elevation, I compute the corresponding shot-side local reference trace as the average amplitude spectrum of all K associated seismic traces with receiver stations located in the Sabkha.

$$U^{I\_shot}(\omega) = \sum_{k=1}^{K} \frac{|S^{IK}(\omega)|}{K}. \quad (3.4)$$

4. After computing all the needed reference traces $U^{gref}(\omega)U^{I\_shot}(\omega)\ and\ U^{J\_rec}(\omega)$, I computed the frequency-dependent de-amplification factor for each receiver and shot station by spectral division, and derived the surface-consistent source and receiver amplification correction factors, respectively, as follows:

$$AMPF^{I\_shot}(\omega) = \frac{U^{I\_shot}(\omega)}{U^{gref}(\omega) + \varepsilon} \quad (3.5)$$

$$AMPF^{J\_rec}(\omega) = \frac{U^{U^{J\_rec}}(\omega)}{U^{gref}(\omega) + \varepsilon} \quad (3.6)$$

The white noise term "ε"=.001 is added to prevent instability of the spectral deconvolution that might give rise from division by zero or very small number.

5. Using equations (4) and (5), I perform the sand dune amplification correction in the frequency domain by taking the Fourier transform of each trace on a dune elevation as follows:

$$S^{ij\_cor}(\omega) = \frac{S^{ij}(\omega)}{AMPF^{I\_shot}(\omega) * AMPF^{J_{rec}}(\omega)} \quad (3.7)$$

Where $S^{ij}(\omega)$ and $S^{ij\_cor}(\omega)$ are the Fourier Transform of a seismic trace before and after correction of Sand Dune Amplification effects respectively. Performing an inverse Fourier transform on $S^{ij\_cor}(\omega)$ yields the seismic trace in the time domain.

Before describing examples, it is worth considering the validity of the assumptions made in this method. In the actual computation of the global reference traces, the amplitude spectra of the traces from the Sabkha are averaged when calculating the correction factor. The method assumes that the averaging algorithm will smooth out the short-term and local fluctuations between stations, and highlights the global long-term fluctuations. Therefore, the method assumes that any spectral differences observed between the global trends and sand dune stations are due to local effects of sand dunes. Figure 3.1a compares the local reference traces of three stations positioned on top of the sand dune with three stations positioned on the Sabkha. In general, the amplitude spectrum of the dune stations is variable and shows much higher amplitudes across the entire frequency spectrums than those of the Sabkha stations. Small variation exists between the Sabkha amplitude spectrums, which are assumed to be smoothed out in the global reference trace. Figure 3.1b, shows the same comparison for the field data.

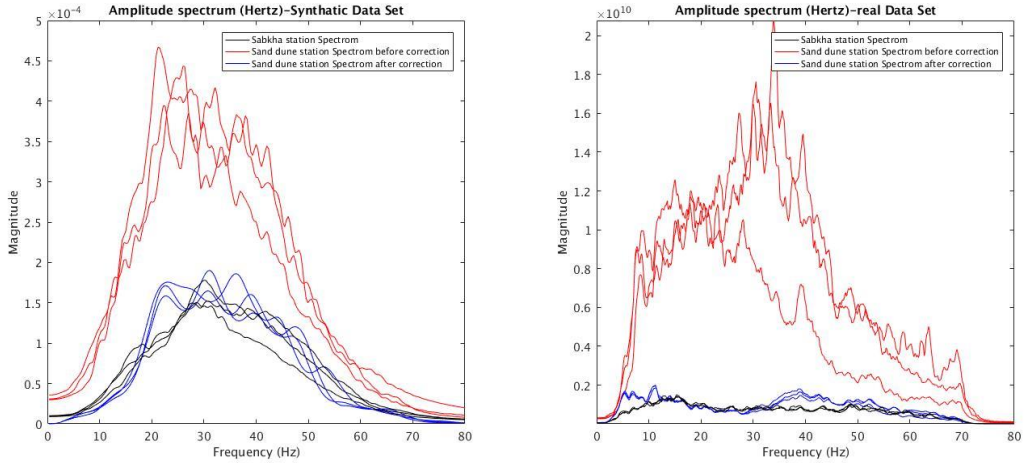

(a) (b)

Figure 3.1. The average amplitude spectra associated with several stations for synthetic (a) and real data sets (b). The entire trace was used to compute the average amplitude spectra of the traces corresponding to each station. The black curves represent the average amplitude spectra for stations positioned in the Sabkha, while the red and blue curves represent the average amplitude spectra of sand dune stations before and after application of the amplitude correction respectively.

CHAPTER 4

NUMERICAL SIMULATION

4.1 Model parameter

In this study, I ran an elastic simulation to investigate the sand dunes effect using an optimized finite-difference modelling scheme proposed by Etienne et al. (2007) to assess the performance of the new scheme developed at Saudi Aramco.

The scheme uses the second-order wave equation and a higher order scheme in space. The model parameters used in the scheme are given in Table 4.1. The simulation used standard staggered-grid (SSG) and perfectly matched layer (PML) boundary conditions. To ensure a total absorption for incoming waves, the PML boundary used 60 grid points in width. The model domain has 601 × 2001 grid points with 1 m grid spacing along the vertical and horizontal axes. The time step was set at 0.02 milliseconds to ensure numerical stability according to the Courant criterion. The total recording time simulated was 2 s to ensure that a lot of the noise was recorded. The model was simulated 1000 times with the source at a different location at 2 meters apart. The sources were placed at a depth of 1 m below the surface. The source type used was a vertical source and the source wavelet is a Ricker wavelet with a central frequency of 50 Hz (Figures 4.1). The central frequency is within the range normally used for exploration seismic. Receiver positions were defined along one line in the computational domain. The spacing is 1m and the receiver line consists of 2000 receivers. For all models, the receivers' vertical placement follows the topography.

The lines start at x=1 m and continue to x=2000 m; the y coordinate stays the same. The outputs from the simulations were shot gathers of the particle velocity in the z direction.

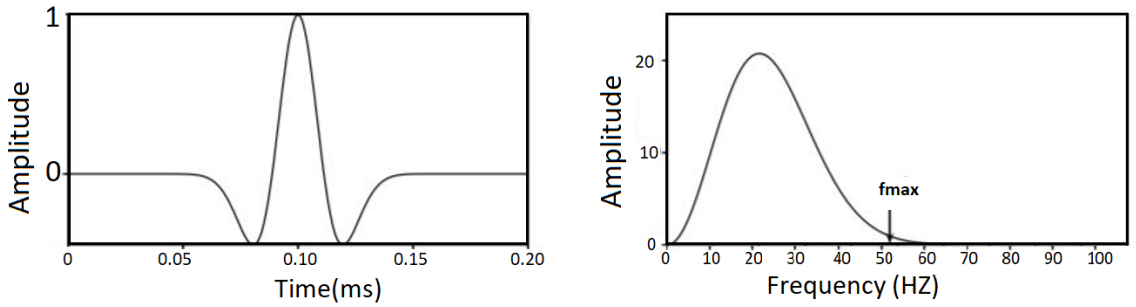

Figure 4.1 The wavelet shape in time domain (a) and the corresponding frequency amplitude spectra (b).

4.2 Model Design

I simulated a four-layer model (air, Sabkha, and two clastic layers) with a circular feature on the surface to represent a sand dune (100 m high and 200 m wide), as shown in Figure 4.2. Only four layers are used in the simulation to keep the complexity of the deeper layers to minimum. This doesn't reflect the reality but as the main focus of the study is to investigate the sand dunes effects on the data, adding more layers will only create unnecessary complexity. Although the dunes are heterogeneous in reality (Robinson & Al-Husseini 1982), I assumed a homogeneous model for the dune because the developed methodology is mostly concerned with correcting the amplification generated by the high acoustic impedance between the Sand dune and Sabkha. The P-wave velocity values for the sand dunes and Sabkhas were taken from literature (Al-Shuhail & Al-Shaibani, 2009; Liner, 2008). A P-wave to S-wave velocity ratio of 2 were used for the sand dune layer

and 1.73 for the rest of the layers. The model domain has 601 × 2001 grid points with 1 m grid spacing along the vertical and horizontal axes. I generated shot records over the entire model with 2 m shot spacing. Each shot was generated for the same receiver layout covering the extent of the model, with 1 m receiver spacing.

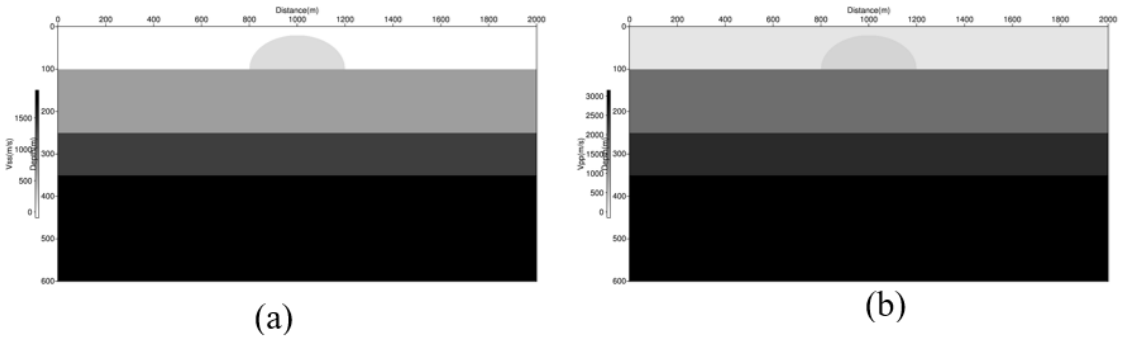

Figure 4.2 S-wave (a) and P-wave (b) 2D velocity model consisting of a four-layer model (air, Sabkha, and two clastic layers), with an ellipse-shaped hill layer that represents sand dunes.

Table 4.1 Modeling parameter

	Vp	Vs
Air layer	300	0
Sand dunes	500	250
Sabkha	1700	800
Clastic	2500	1500
clastic2	3000	1850

Spatial grid dimension	1 meter
Time step	$2x10^{-4}$ ms
Source function	Ricker wavelet
Maximum frequency	50 Hertz

Number of shots	1000
Number of receivers	2000
Source interval	2 meters
Receiver interval	1 meter

4.3 Results

Figure 4.3 shows the simulation results for the first shot record; shot placed at x=0, where some events were distinguishable (i.e. direct wave, ground–roll forming a shadow cone, and P-wave reflection and refraction events). I note that the traces from stations in the simulation located over the dune exhibited large static shifts, much higher amplitudes, and lower S/N compared with traces collected in the Sabkha.

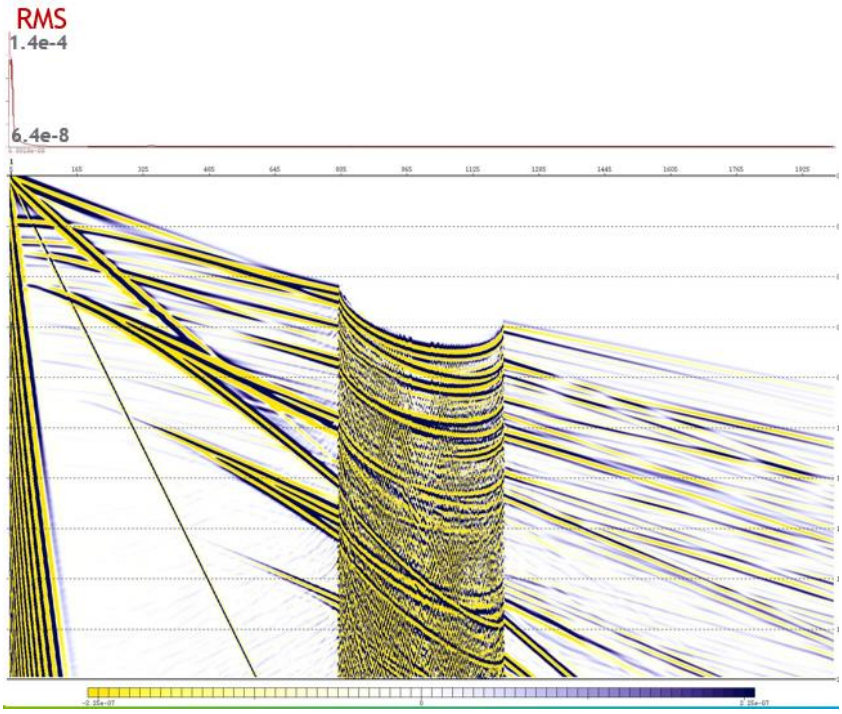

Figure 4.3 The result of running the simulation source placed at 1 m. The red curves on the top represent the corresponding RMS amplitude.

Figure 4.4 shows the same shot record after performing the sand dune amplification correction. For this synthetic example, I computed the reference traces using the same fold and offset range (200–800 m). Overall, the correction attenuated the amplification effects caused by the dune. The amplitude variation in the offset direction was more consistent with the trend observed on a shot record without the dune on the surface. I observed a significant S/N ratio improvement on traces from the sand dune environment after the amplification correction, although static corrections are needed to correct the time shifts induced by the low velocity of the sand dune material. In addition, the traces from stations located over the dune exhibited a more consistent RMS amplitude after the application of the amplitude correction trend, compared with traces collected in the Sabkha.

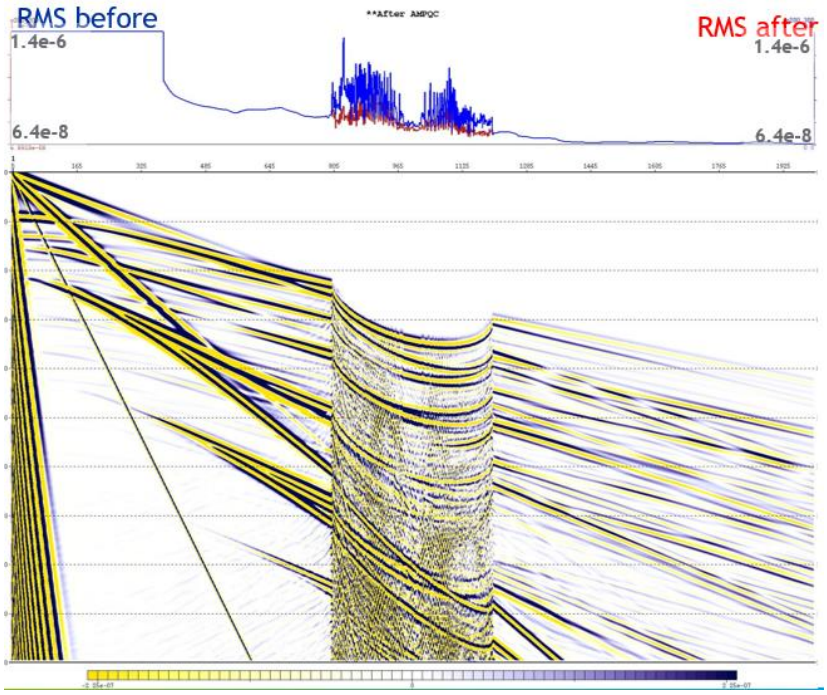

Figure 4.4 The same record as Figure 4.3 after sand dune amplification correction. The blue and red curves on the top represent the corresponding RMS amplitude before and after application of the amplitude correction, respectively. A threshold of .000015 was placed on the RMS computation of the near offset traces.

Figure 4.5 compares the local reference traces of three stations, synthetic data set, positioned on top of a sand dune with three stations positioned on the Sabkha. In general, the amplitude spectra of dune stations are variable and show greater amplitudes across the entire frequency spectra than those of the Sabkha stations. Small variations exist between the Sabkha amplitude spectra, which I assume are smoothed out in the computation of the global reference trace.

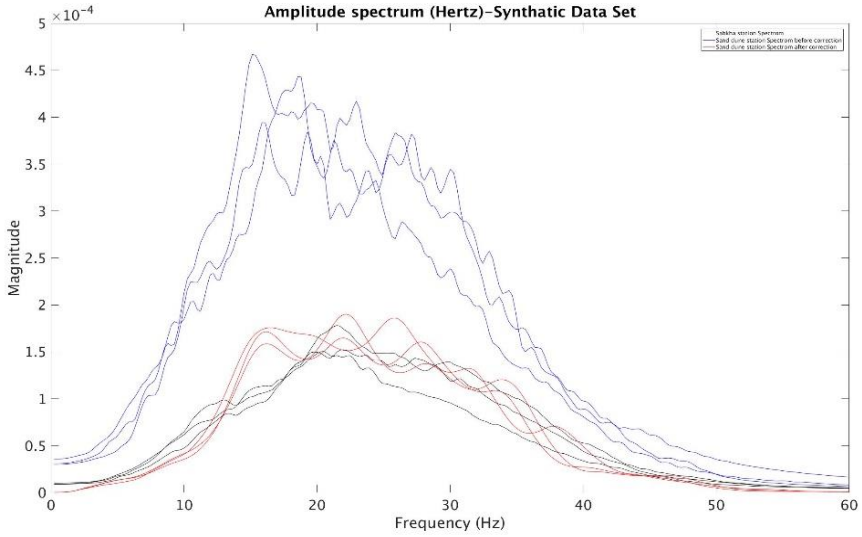

Figure 4.5 The average amplitude spectra associated with several stations for synthetic (a) and real data sets (b). The entire trace was used to compute the average amplitude spectra of the traces corresponding to each station. The black curves represent the average amplitude spectra for stations positioned in the Sabkha, while the red and blue curves represent the average amplitude spectra of sand dune stations before and after application of the amplitude correction respectively.

CHAPTER 5

REAL DATA ANALYSIS

In this chapter, I introduce the acquisition parameter for the field data set which is used to test the new methodology. In addition, I examine the effects of using a different operator design window. Furthermore, the amplification as a function of soil thickness and offset is also examined.

5.1 Acquisition parameter for the 2D real data set

Ideally, the global and local reference traces should be computed from traces with similar offsets that consistently cover the dune and Sabkha areas. This is not achievable with actual data in part because of the challenging terrain conditions and the fact that data acquisition is not designed to optimize offset distribution for amplification correction. Therefore, a proper analysis of the field parameters is essential for the success of the amplitude amplification correction. The offset histogram is presented in Figure 5.1. The survey consists of 7000 receivers, out of which 2000 are affected by the sand dunes. The total number of shots is 7000, with 1200 traces per shot that corresponds to a total of 54000 traces. Only 16 shots are located on the sand dunes due to the difficulty of setting seismic sources on dune elevations. The total number of traces affected by the sand dunes is 23222 (either the receiver, source or both were affected by sand). The offset histogram of the Sabkha traces shows how the count number of traces decrease with the offset. To derive a non-biased reference trace with regards to offset, it is critical to ensure that the traces forming the global reference trace have the similar offset range. Note that, the

survey has more near offset traces. Accordingly, the inclusion of near offset traces in the operator design window will bias the computation.

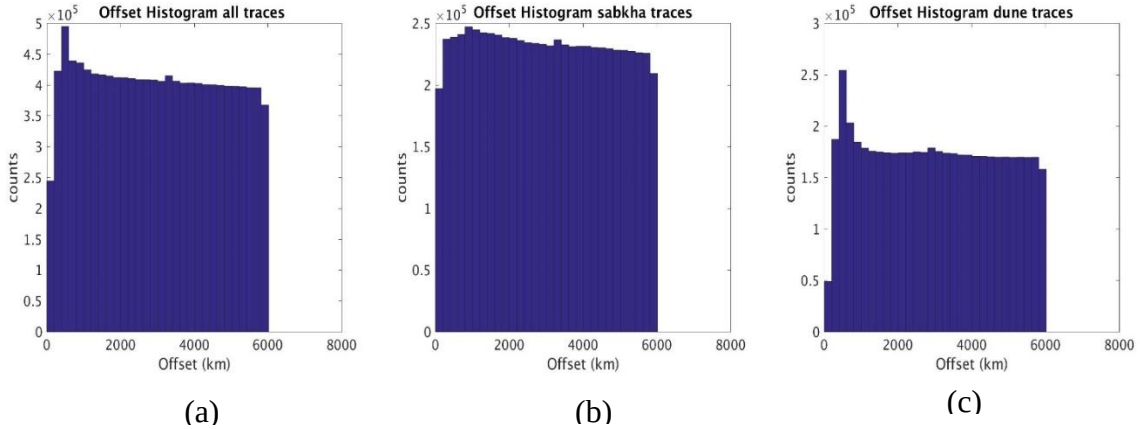

Figure 5.1 Histogram of offset distributions within a seismic survey. (a) All the traces, (B) and (C) the Sabkha and dune traces respectively.

5.2 Operator design window

I calculate the global reference trace spectrum using different offset ranges to investigate its effect. Figure 5.2 shows the Global Reference Trace (GRT) spectra for a wide range of offsets. The amplitude spectrum of the GRT using smaller offset ranges, e.g. 0–1000 m, is higher across the entire frequency band than those with a larger offset that ranges of 0–6000 m and 3000–6000 m respectively. It is also observed that the small offset ranges show a much higher amplitude across the whole frequency spectrum than the far offset ranges as expected.

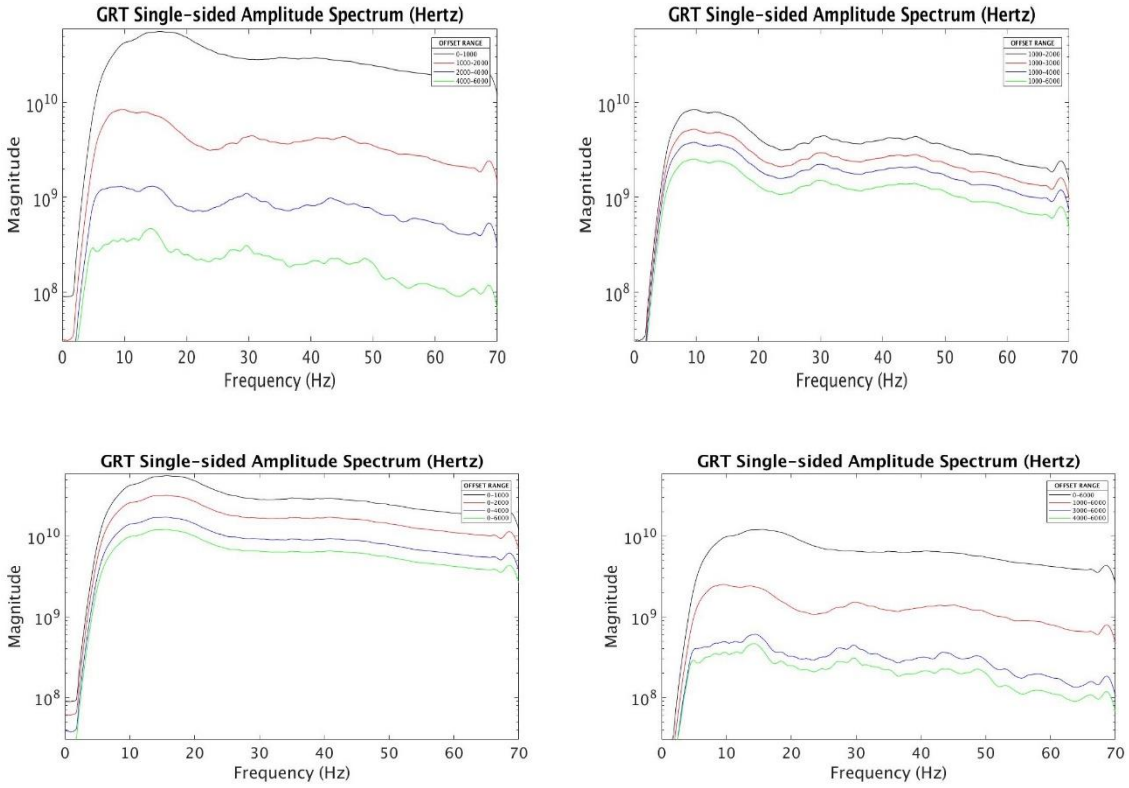

Figure 5.2 The GRT spectra using different range of offsets. The graph is displayed with frequency-x-axis, in Hertz, and a log-amplitude y-axis.

Figure 5.3 shows the amplification correction of traces at different offset ranges. The input seismic trace is shown in the first panel of the figure. The output traces using a correction factor that included the near offset traces, e.g. for 0–1000 m, 0–6000 m, lengths overcorrected (de-amplified) the near offsets traces. Also, I observed that the correction factor derived using the range of far offset traces (e.g. for 3000–5000 m, 300–6000 m) resulted in a moderate amplification correction as evidenced by the consistent amplitude trend. Therefore, I conclude that an amplification correction derived using the 3000–5000 m offset range is appropriate for this study.

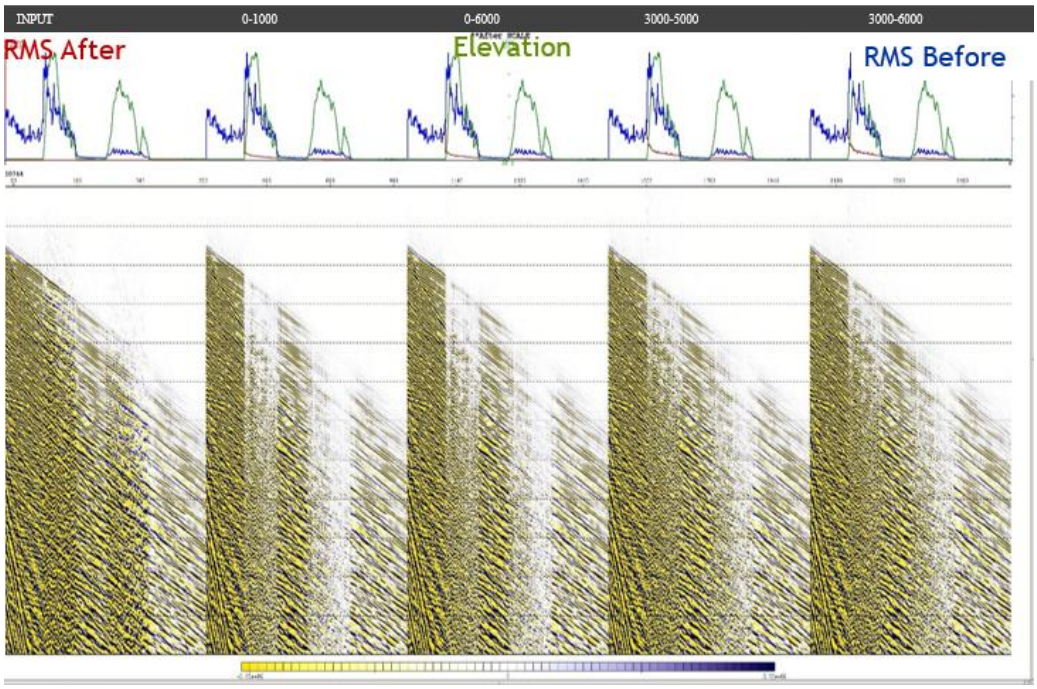

Figure 5.3 The effects of choosing a different offset range for computation of the sand dune amplification correction for the shot gather. The green curve on the top represents the sand dune elevation in mater, and the red and blue curves represent the RMS amplitude before and after the application of the sand dune amplification correction respectively.

5.3 Amplification as a function of soil thickness

In this section, I assume that the sand dunes in the Rub Al-Khali region are relatively uniform in stiffness, so variation in dune thickness led to the observed large level of amplification. In Figure 1.2, I observed that the average amplitude spectrum of 20 traces, with different soil thickness, displayed different level of amplification. To investigate the correlation between the soil thickness and the amplification, I performed the following steps:

(1) Compute the local reference traces for all the sand dune stations in my survey using equation 3.3.

(2) Compute the mean amplitude spectrum between 0 to 60 Hz for all the sand dune stations.

(3) Plot the average amplitude spectrum for each station with the corresponding statics corrections.

(4) Create a linear regression line fit to the data.

Figure 5.3 shows the average amplitude spectrum for the sand dune stations, the corresponding statics corrections and the fitted linear regression line. Note that the static corrections along this seismic line are purely caused by the sand dunes. Consequently, a higher static correction value corresponds to a thicker sand dune deposit. From Figure 5.3, it is apparent that there is a positive correlation between the soil thickness and the average amplitude spectrum. The coefficient of determination of the fitted line is 0.873 in Figure 5.3. Though I would need to consider information such as the number of stations per soil thickness to make an accurate statistical prediction as to how well the regression line represents the true relationship, nevertheless I can generally say that the presence of a thicker sand dune thickness corresponds to a higher average amplitude spectrum.

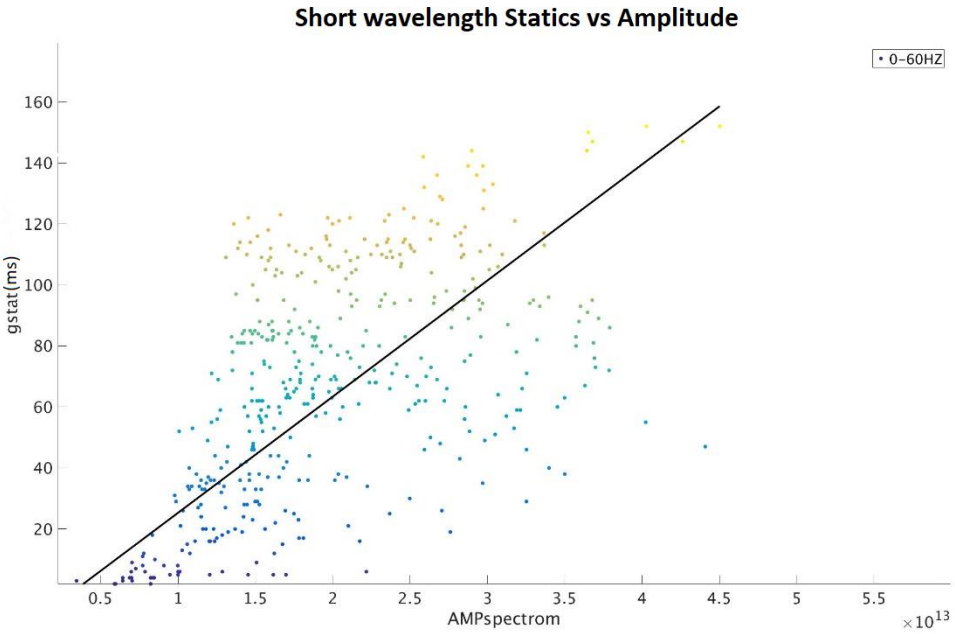

Figure 5.4 the average amplitude spectrum for the sand dune stations verse the corresponding statics corrections with the fitted linear regression line.

Next, I perform the same analysis, using a series of 10-Hz-wide window. Figure 5.5 shows the regression lines associated with different frequency bandwidths. I observed a steeper slope for the regression lines created using lower frequency bandwidths. This suggests that for the sand dune stations, the lower frequencies will generally exhibit higher amplitudes.

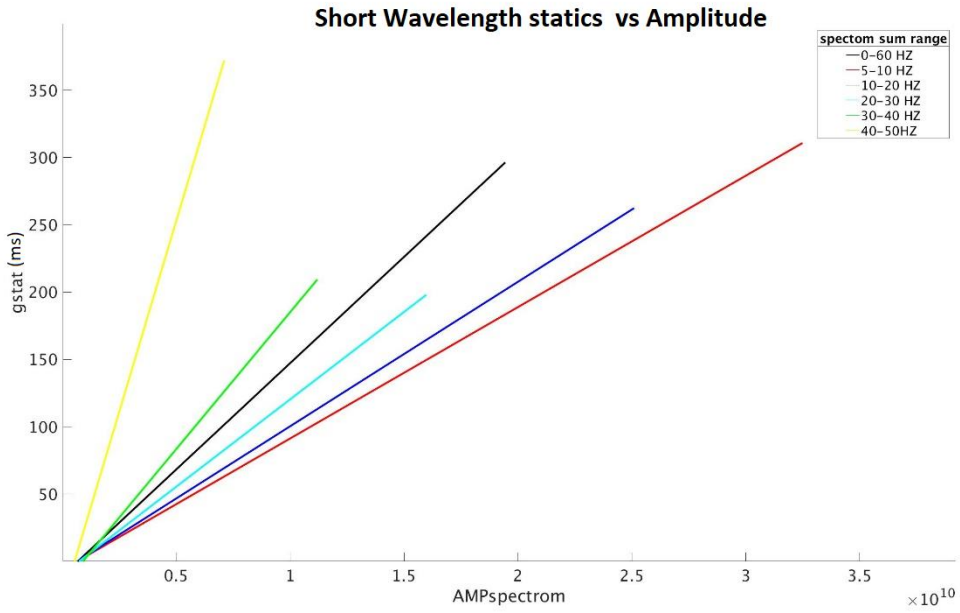

Figure 5.5 The regression lines associated with different series of 10-Hz-wide window for averaging the amplitude spectrum and the corresponding statics corrections.

5.4 Amplification as function of offset

In this section, I analyze the relationship between the amplitude spectra and the offset by averaging the amplitude spectrum off all the sand dunes traces and all the Sabkha traces within different offset ranges (Figure 5.6). Note, that averaged sand dunes spectra showed much higher amplitudes across the whole frequency spectrum than the averaged Sabkha spectra. However, it appears that the difference in the amplitude spectra shape beyond 1000 m is more significant; whereas, it becomes less evident at the very near offset ranges. Note that the amplitudes of higher frequency components suffered from greater attenuation over the same distance than did the lower frequency components. Furthermore, the low frequency attenuation is greater in the Sabkha sediments in comparison to the sand dunes sediments in all offset ranges.

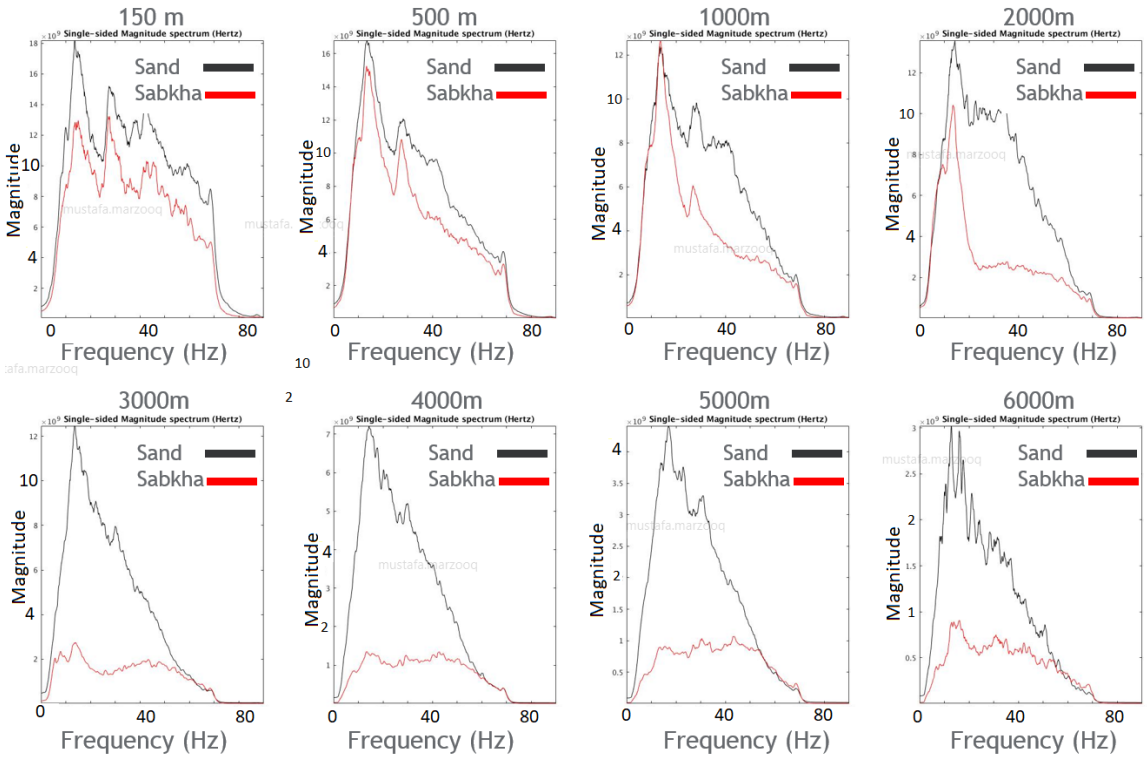

Figure 5.6 Comparison between the average amplitude spectrum between the Sabkha traces, in red, and the sand dune traces, in blue, at different offset ranges.

5.5 Resonance frequency

As I have shown in section 2.3, the degree of the amplification is affected by the reverberations (resonance) of seismic waves within the soft sedimentary cover at the soil natural frequency. For a layer with a rigid interface at the bottom and a free-surface at the top, the relationship between resonance frequency and soil thickness as well as velocity can be approximated by equation 1.1. Robinson and Al-Husseini (1982) developed an empirical relationship between the transit time of P-waves in sand and the thickness of dunes. They used that relationship, commonly known as the sand curve method, to derive sand dune statics for seismic data from the Rub Al-

Khali region (Figure 5.7). Using the sand curve and equation 1.1, I created an empirical relationship between the sand dunes thickness and the resonant frequency (Figure 5.8).

Note that according to the resonant frequency curve, there is negative correlation between the soil natural frequency value and the thickness of the sand dunes, which is in agreement with the physics of 1D resonance (Brad & Bouchon 1985). In other words, vertically travelling waves with lower frequencies have a tendency to be tuned to thicker sand deposits.

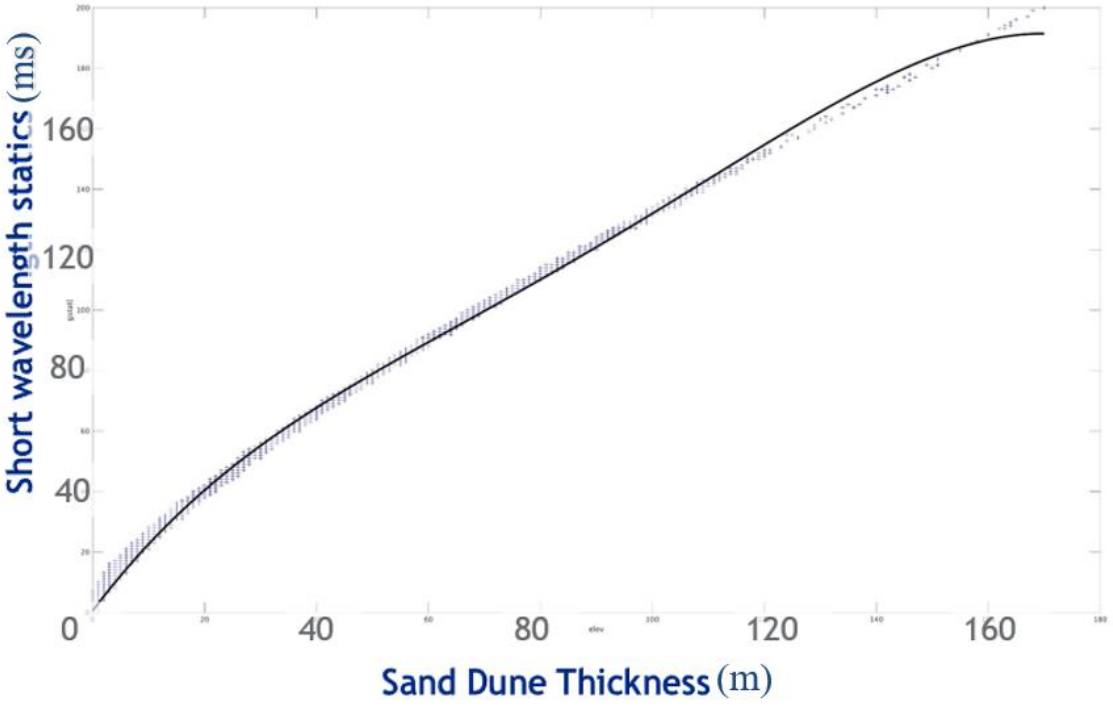

Figure 5.7 Sand Curve (Robinson & Al-Husseini 1982) gives the transit time of P-waves in sand and the thickness of dunes.

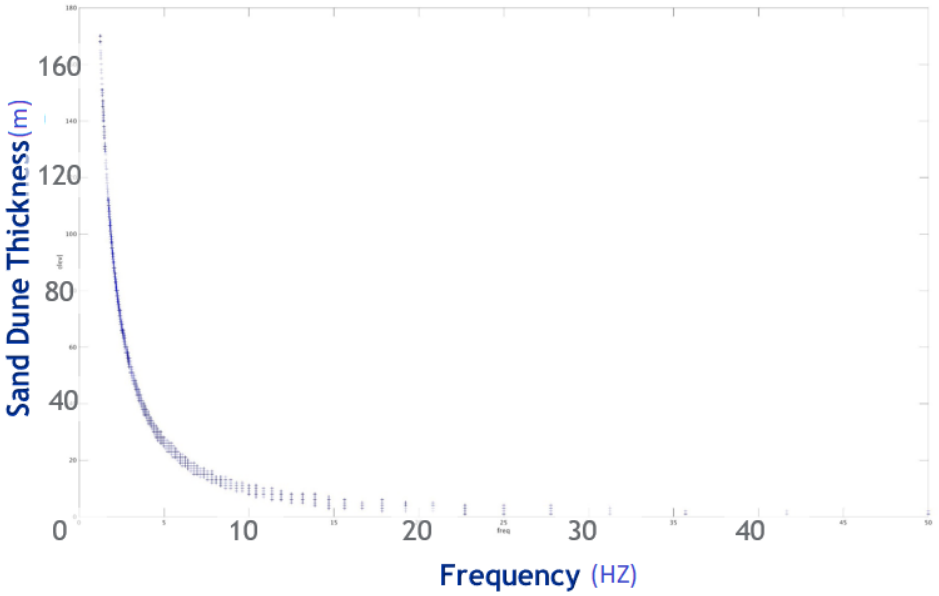

Figure 5.8 Resonance curve: gives the soil natural frequency of the sand and the thickness of dunes.

Using the resonant curve, I compute the corresponding resonant frequency for each station in my survey. Figure 5.9 and Figure 5.10 compare the computed resonant frequency and the observed resonant frequency as well as the peak of the average amplitude spectra per station, for different sand dune structure in the survey. I observed that although there is a mismatch between the computed and observed soil natural frequency value, the curve shape is similar. The disagreement in the frequency value between the observed and computed is attributed to the approximation I made in equation 1.1, which assumes a simple 1D layer. In addition, the predominant frequency of the recorded signal is highly influenced by the frequency content of the input motion (Mondal & Kumar, 2015). The vibrator sweep, 6 Hz to 80 Hz, doesn't extend to the low frequency end.

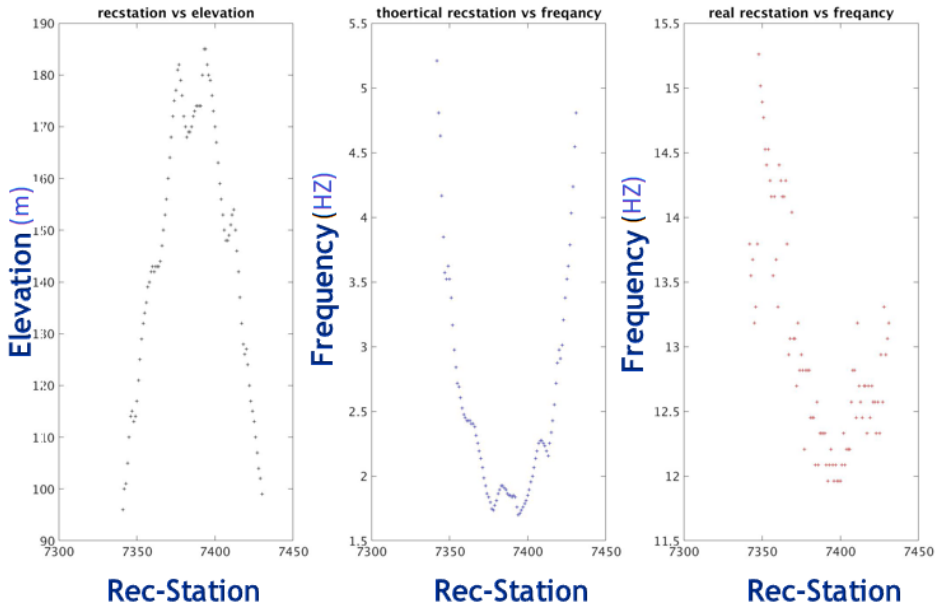

Figure 5.9 A comparison between the theoretical and observed resonant frequency for receiver stations 7300-7450. (a) The Elevation profile (b) the computed and observed (c) resonant frequency.

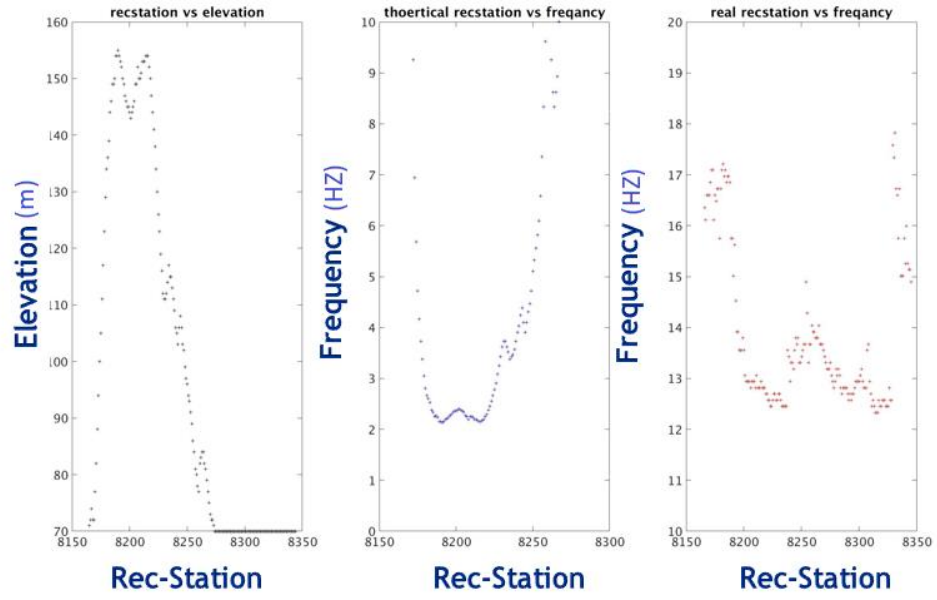

Figure 5.10 A comparison between the theoretical and observed resonant frequency for receiver stations 8150-8350. (a) The Elevation profile (b) the computed and observed (c) resonant frequency.

CHAPTER 6

METHODOLOGY APPLICATION

After validating our new methodology on synthetic data, I applied it to actual 2D seismic data. The acquisition parameters for this dataset are summarized in Table 2. The Sabkha floor for this analysis was located 75 m above sea level, and the sand dune elevation was between 0–125 m above the Sabkha floor. I found that the static corrections along the seismic line were solely caused by the sand dunes and reached a maximum of -210 millisecond. The static corrections were computed using the sand curve method (Liner, 2008). Figure 6.1 shows a raw shot record with and without the static corrections application. The record is characterized by the low-frequency ground roll and the backscattered events generated by the rough dune topography. I also observed that traces collected from stations located over the dune exhibited large static shifts, higher amplitudes, and lower S/N compared with traces collected in the Sabkha. Static corrections were successful in removing the misalignment caused by the near surface and improving the focusing and continuity of the events. More enhancements are expected with the application of the surface-consistent residual statics.

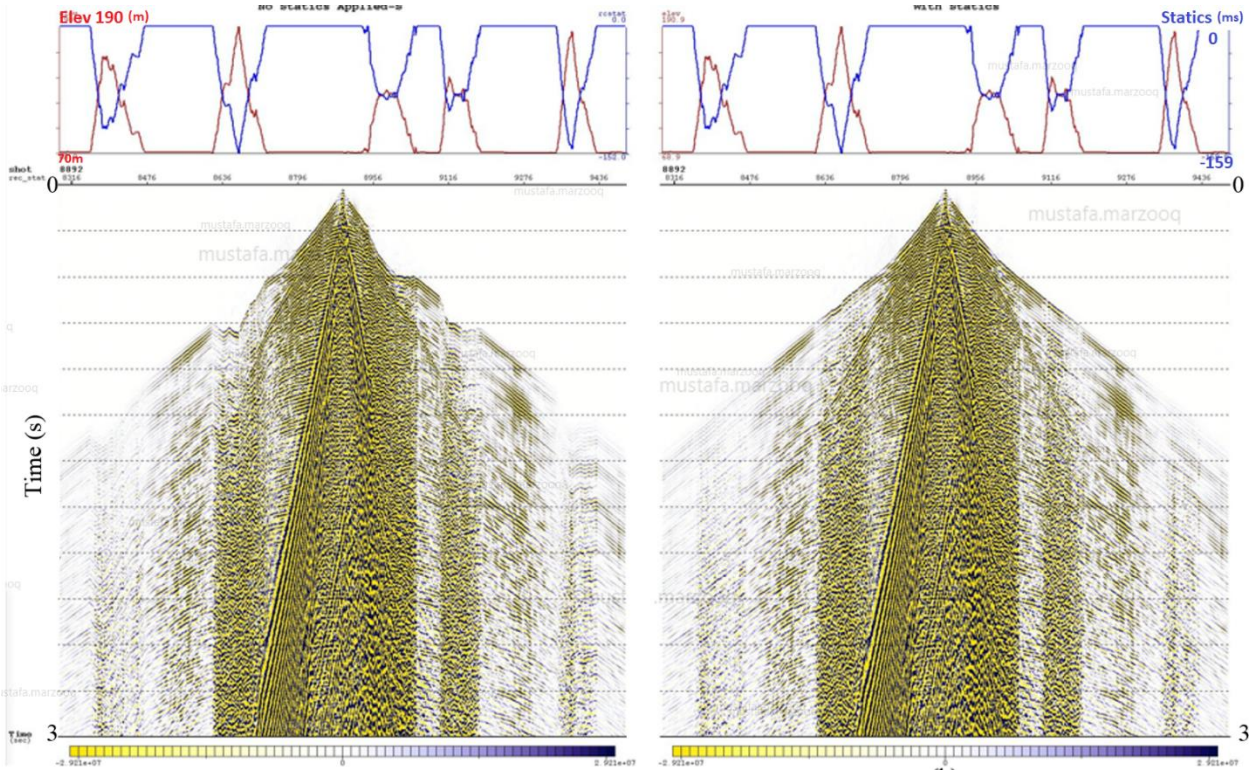

Figure 6.1 Representative shot gathers. a) A raw field record with geometric spreading correction applied. b) The same record as Figure 6.1a after the application of statics correction. The red curve at the top represents the elevation.

The effect of the sand dune amplification correction is illustrated in Figures 6.2 and 6.3, which show traces collected in a common shot gather before and after the correction. The first panel in Figure 6.1 represents field data without any filter applied. The two records were filtered using a series of 20 Hz-wide bandpass filters. The differences between the traces in the gathers are noticeable. In the raw common shot gathers, the traces between 300 m and 800 m, received by a geophone positioned in the sand dunes, exhibit much higher amplitudes and lower S/N compared with the traces collected in the Sabkha. Figure 6.3 shows the same shot record as Figure 6.2 after performing the sand dune amplification correction. Overall, the correction reduced the

amplification effects caused by presence of the dune. Following the correction, the amplitude variation in the offset direction is more consistent with the trend observed on a shot record without the dune on the surface, and I observed a significant improvement in the S/N of traces from the sand dune environment. More importantly, the traces collected in the Sabkha were not altered by the de-amplification step. When the filter panels in Figure 6.2 and 6.3 were compared with the same frequency band, I observed that the sand dune amplification correction brought the signal down for the entire recording time. However, the amplification correction did not reduce amplitudes of the high frequencies as much as it did for low frequencies because the low frequencies exhibited much stronger amplification. The corresponding frequency wavenumber (F-K) spectra to these data are shown in Figure 6.4. I computed these spectra using traces ranging between1200–6000 m. By selecting one side of the shot, I interpreted energy corresponding to a negative wavenumber as noise was generated by the scattering and reverberation. The results are shown with the same scale. The spectra demonstrate that, following the correction, I successfully attenuated scattered energy caused by the presence of the dune, allowing the signal and surface wave to be more visible.

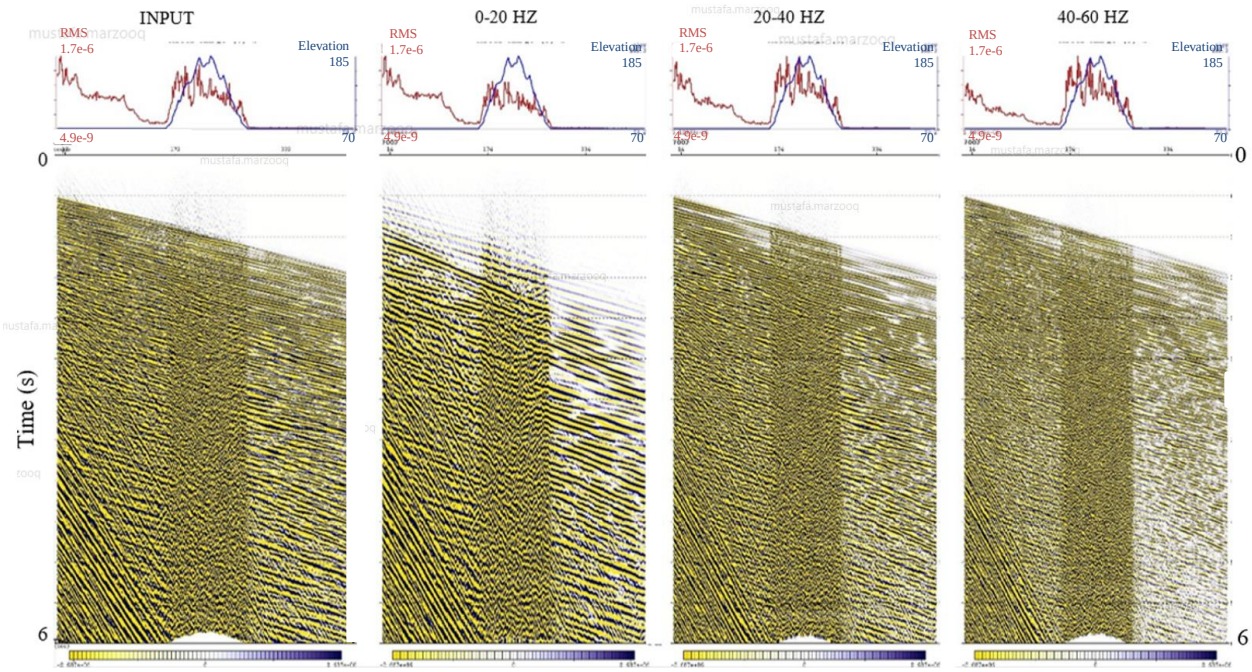

Figure 6.2 A raw field record with spherical divergence correction (far left panel) and its bandpass-filtered versions. The blue and red curves on the top represent sand dune elevation and the RMS amplitude, respectively. Note the amplification and a low S/N in the traces collected in the sand dunes.

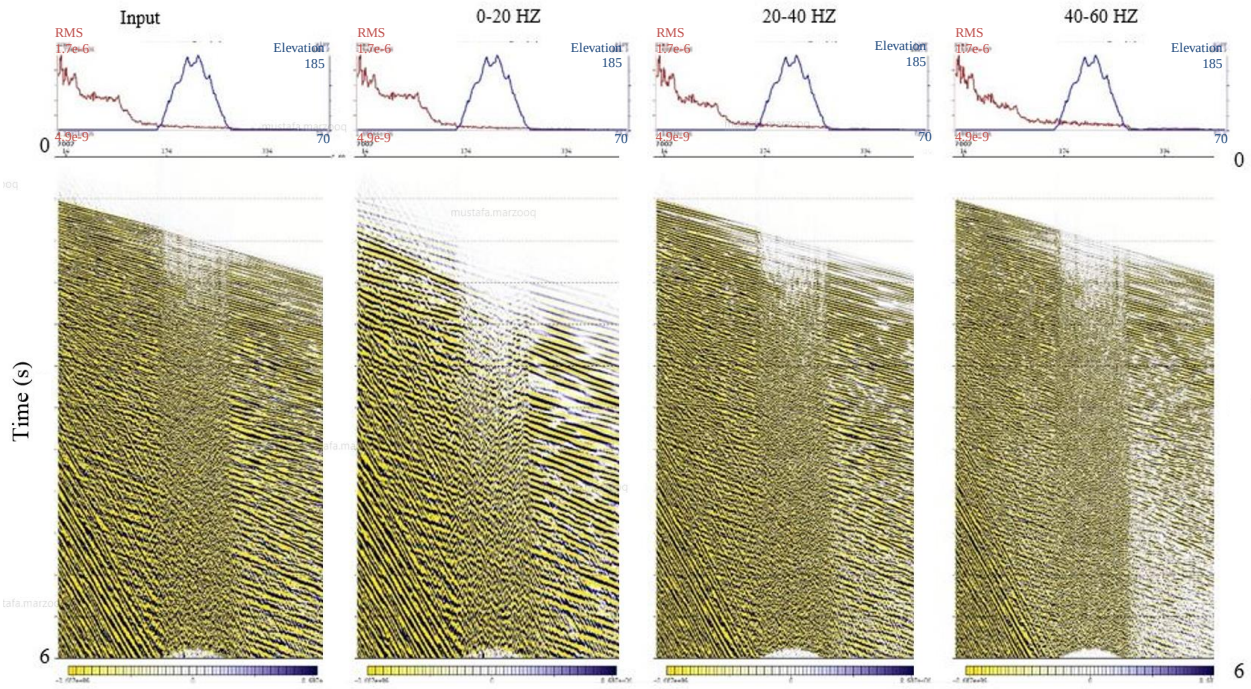

Figure 6.3 The same field record as in Figure 6.2 and its bandpass-filtered versions following application of the sand dune amplification correction. The blue and red curves on the top represent the sand dune elevation and the RMS amplitude, respectively.

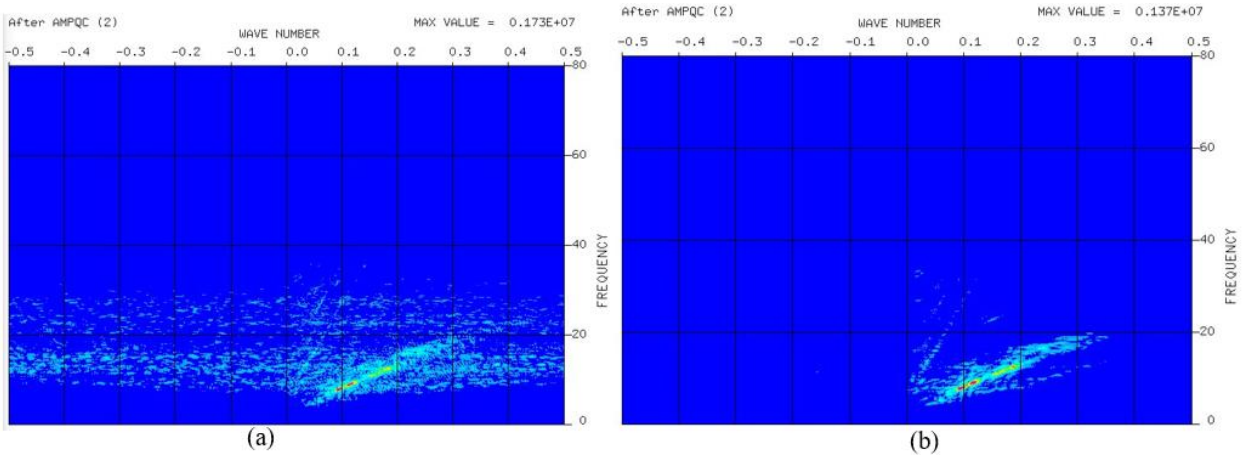

Figure 6.4 The corresponding F-K spectra for data shown in Figure 9a and Figure 10a on a decibel scale. The graph is displayed with frequency- y-axis, in Hertz, and wavenumber x-axis, in 1/m; the colors represent the relative energy in decibel.

Figure 6.5 compares the local reference traces of three stations, synthetic data set, positioned on top of a sand dune with three stations positioned on the Sabkha. In general, the amplitude spectra of dune stations are variable and show greater amplitudes across the entire frequency spectra than those of the Sabkha stations. Small variations exist between the Sabkha amplitude spectra, which I assume are smoothed out in the computation of the global reference trace.

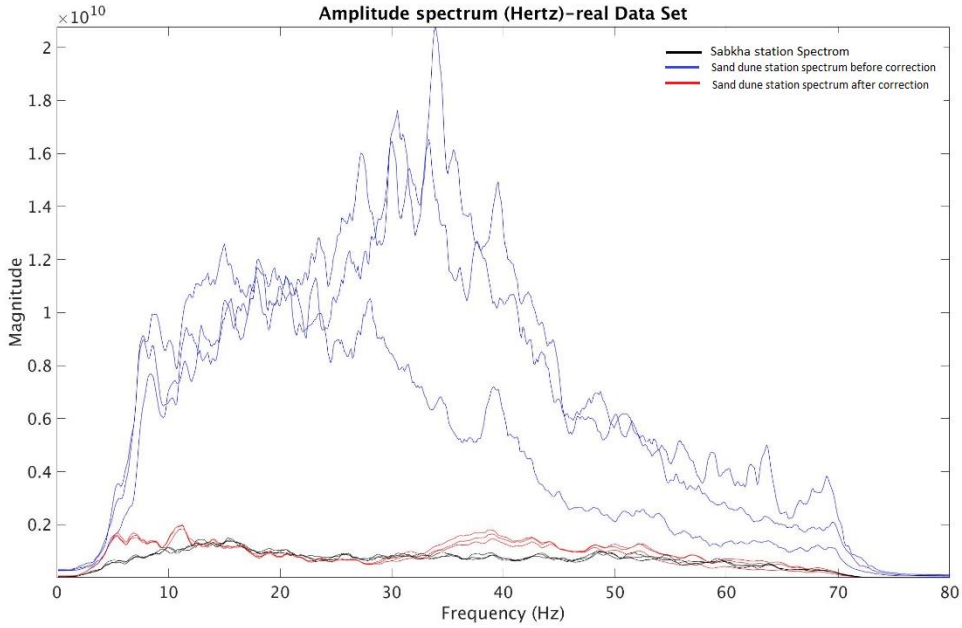

Figure 6.5 The average amplitude spectra associated with several stations. The entire trace was used to compute the average amplitude spectra of the traces corresponding to each station. The black curves represent the average amplitude spectra for stations positioned in the Sabkha, while the red and blue curves represent the average amplitude spectra of sand dune stations before and after application of the amplitude correction respectively.

Figure 6.7, and 6.8 illustrate the scaling problem associated with dune amplification on real data before and after application of amplification correction on a portion of the common offset gathers at near, mid, and far offsets. On top of each section, I plotted the RMS amplitude and the elevation profile. The amplitudes are calculated within a time

window around the first arrival. The RMS amplitudes, prior to application of the amplitude correction, vary by more than a factor of four between the sand dunes and Sabkha traces. This implies that the average reflectivity of the Earth within the RMS amplitude time window varies laterally by this amount. Here, the time section is discontinuous, and the events have inconsistent amplitude variations across the entire section. Anomalous amplification occurs directly in areas of large elevation changes, which correspond to the locations of sand dunes. As shown in the right-side panel of Figures 6.6–6.8, the surface-consistent scaling successfully reduced the relative amplitude variations caused by presence of the dune. The events are better focused after attenuation of near-surface effects associated with the presence of the sand dune.

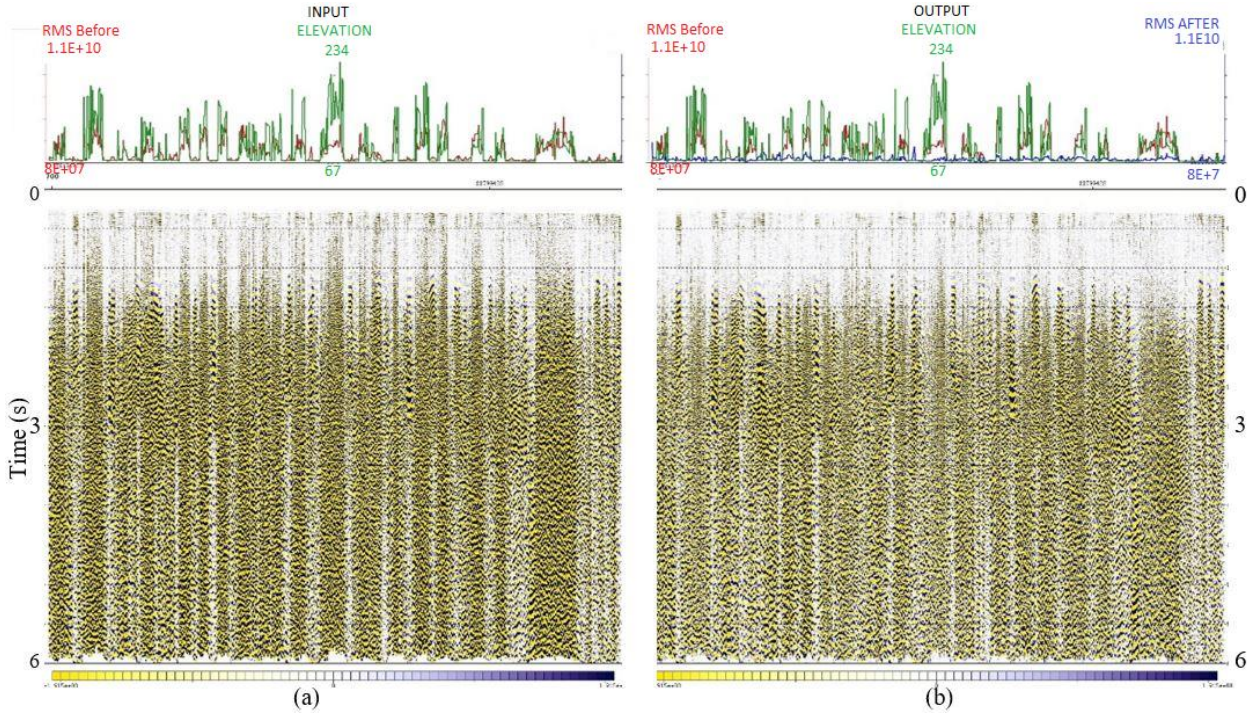

Figure 6.6. Near offset gather for a) only geometric spreading correction, and b) the same record as Figure 6.6a after sand dune amplification correction. The green curve on the top represents the elevation of the sand dune, and the red and blue curves represent the RMS amplitude before and after the application of the sand dune amplification correction respectively.

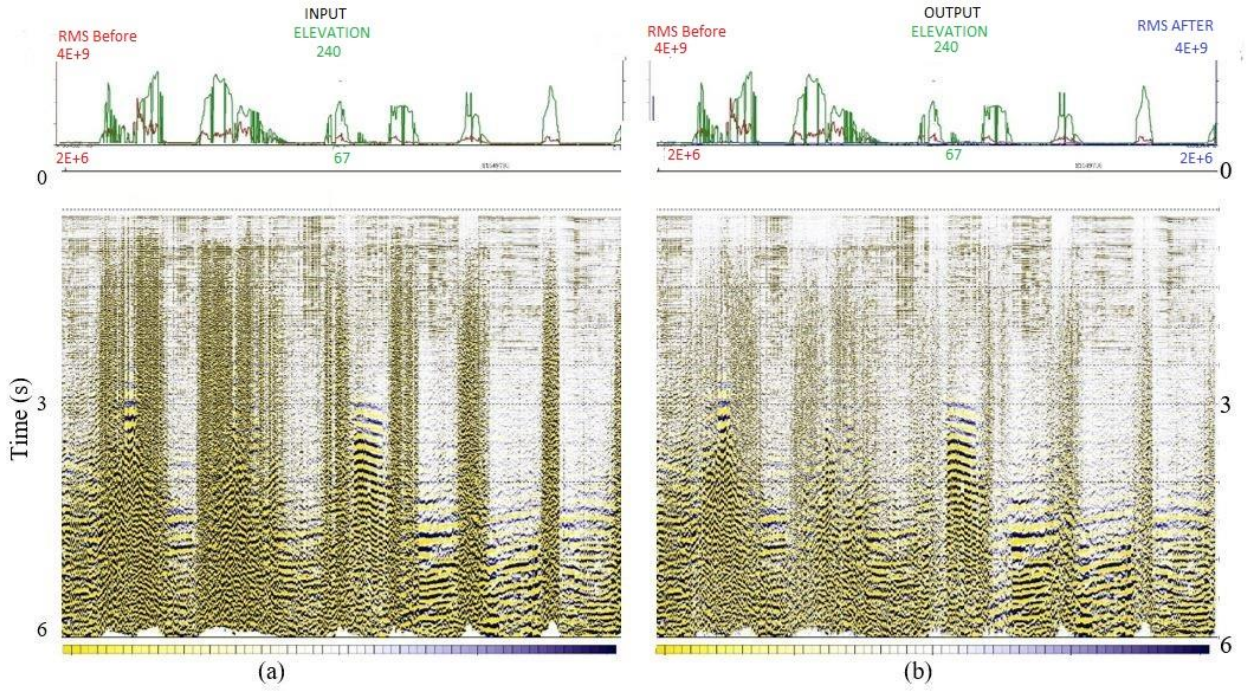

Figure 6.7. Mid offset gather for a) only geometric spreading correction, and b) the same record as Figure 6.7a after sand dune amplification correction. The green curve on the top represents the sand-dune elevation, and the red and blue curves represent the RMS amplitude before and after application of the sand dune amplification correction respectively.

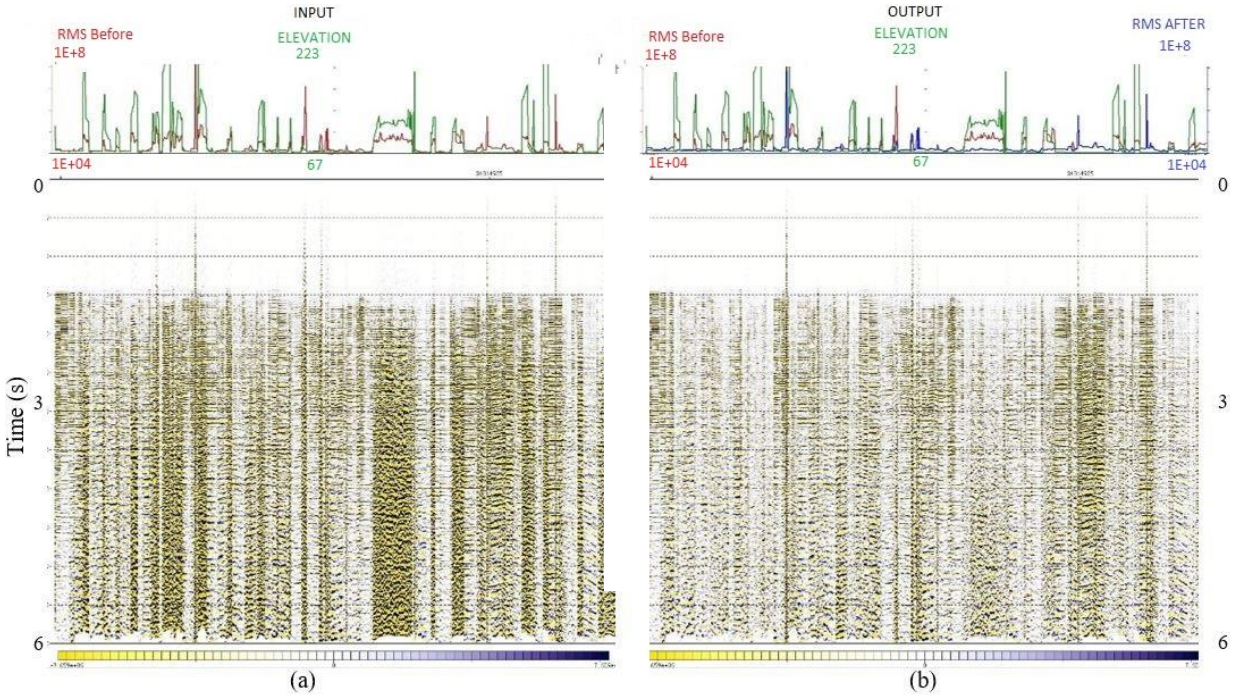

Figure 6.8. Far offset gather for a) only geometric spreading correction, and b) the same record as Figure 6.8a after sand dune amplification correction. The green curve on the top represents the sand dune elevation, and the red and blue curves represent the RMS amplitude before and after the application of the sand dune amplification correction respectively.

To further illustrate the results, Figure 12a and 12b show a common CMP gather, after Normal move out correction and Mute were applied, with and without the sand dune amplification correction. Traces from stations located over the dune, prior to application of the amplitude correction, exhibited different frequency content, much higher amplitudes, and lower S/N compared with traces collected in the Sabkha. Figure 3c shows the same shot record after performing the sand dune amplification correction, now the traces from stations located over the dune exhibited a more consistent RMS amplitude trend, similar frequency and amplitude content compared with traces collected in the Sabkha.

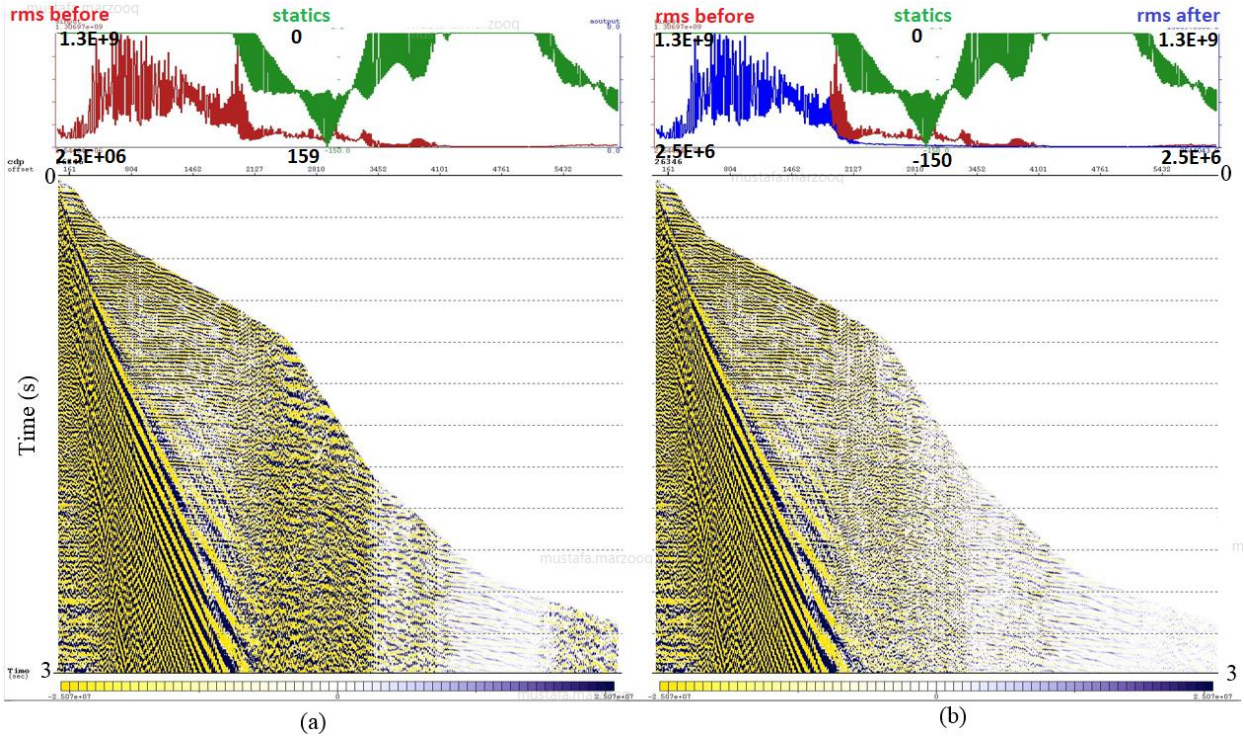

Figure 6.9 CMP offset gather with spherical divergence, NMO and Mute applied (a) and (b) shows the same record as Figure 6.9a after sand dune amplification correction. The green curve on the top represents the short wavelength statics in millisecond, the red and blue curves represent the RMS amplitude before and after the application amplification correction respectively.

I now evaluate the effect of applying sand dune amplification correction on the stack data. The basic stacking sequence includes (1) trace editing; (2) spherical divergence correction; (3) Static correction (4) NMO correction and mute (5) Stacking. The stacked section is shown in Figure 6.10 with and without compensating the application of the proposed method between steps (3) and (4). The elevation and the RMS amplitudes for each trace is plotted on the top of the gather. Before the scaling correction, a spatial amplitude banding was observed on the stack. After the scaling correction, the stacks were better balanced and the near surface effects is accounted for as evidenced by the RMS amplitude that showed more consistent trend which does not reflect the near surface elevation.

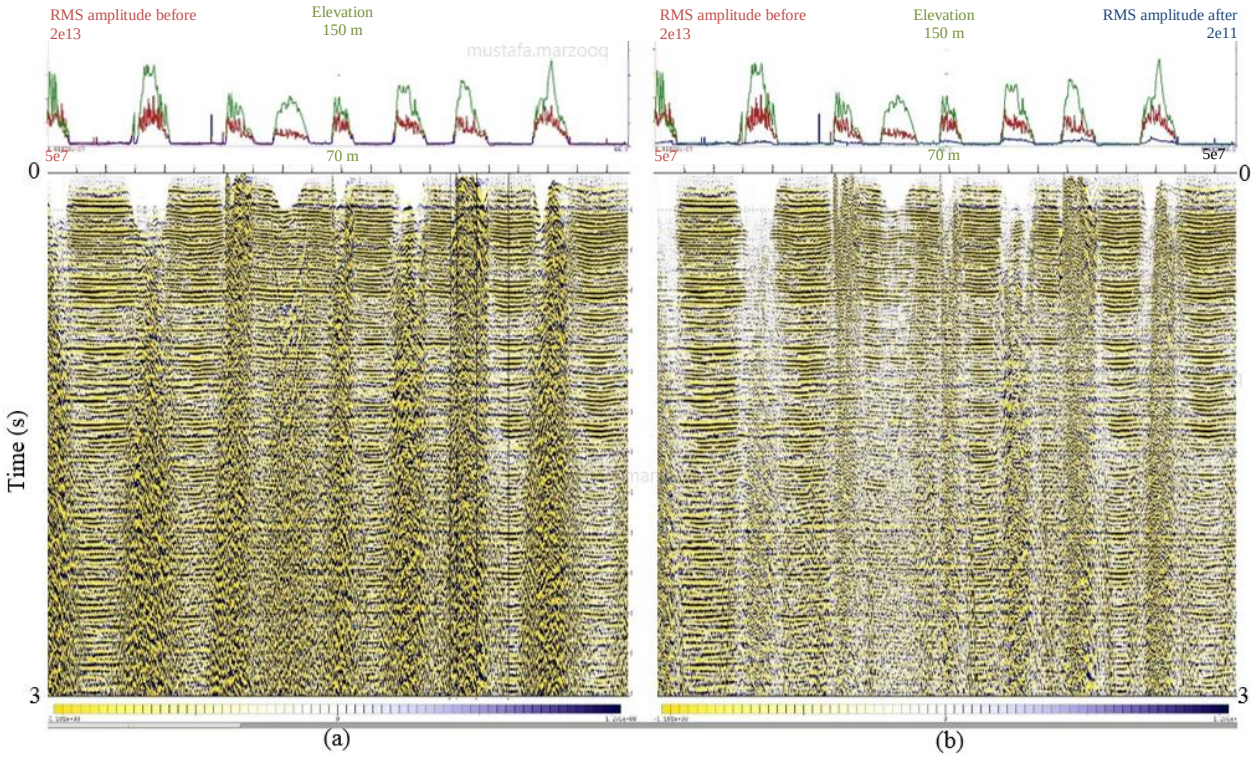

Figure 6.10 A portion of a CMP stack before and after the application of sand-dune amplification correction. The green curve the green curve on the top represents the elevation of the sand dune, and the red and blue curves represent the RMS amplitude before and after the application amplification correction respectively.

To further illustrate the result, I plotted the corresponding amplitude spectra for the first 1000 station prior (Figure 6.11) and after the application of the proposed sand dune amplification correction (Figure 6.12). The observed plunges and upswing in the amplitude spectrum, prior to the correction, correspond to the location of the Sabkha and sand dunes station respectively. Following the correction, the amplitude near surface effects is accounted for and the spectrum showed a more consistent trend, which does not reflect the near surface imprints.

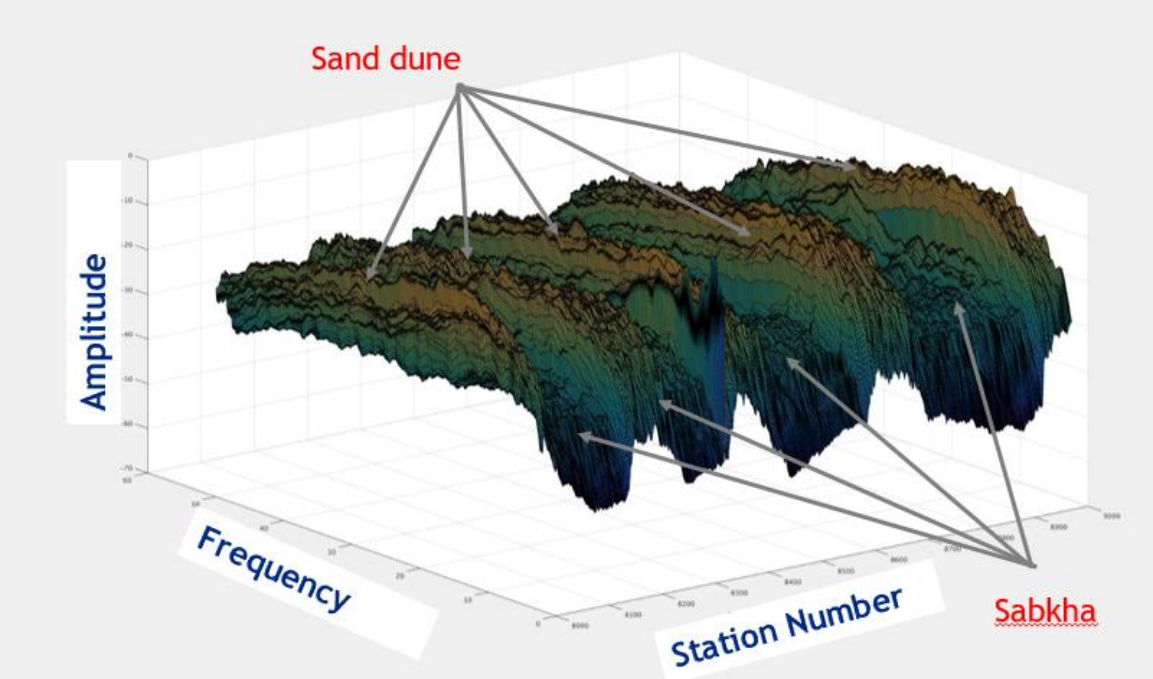

Figure 6.11 The average amplitude spectrum associated with the first 100 stations. The graph is displayed with frequency- y-axis, in Hertz, and station number x-axis; the z-axis represents the relative amplitude energy in decibel.

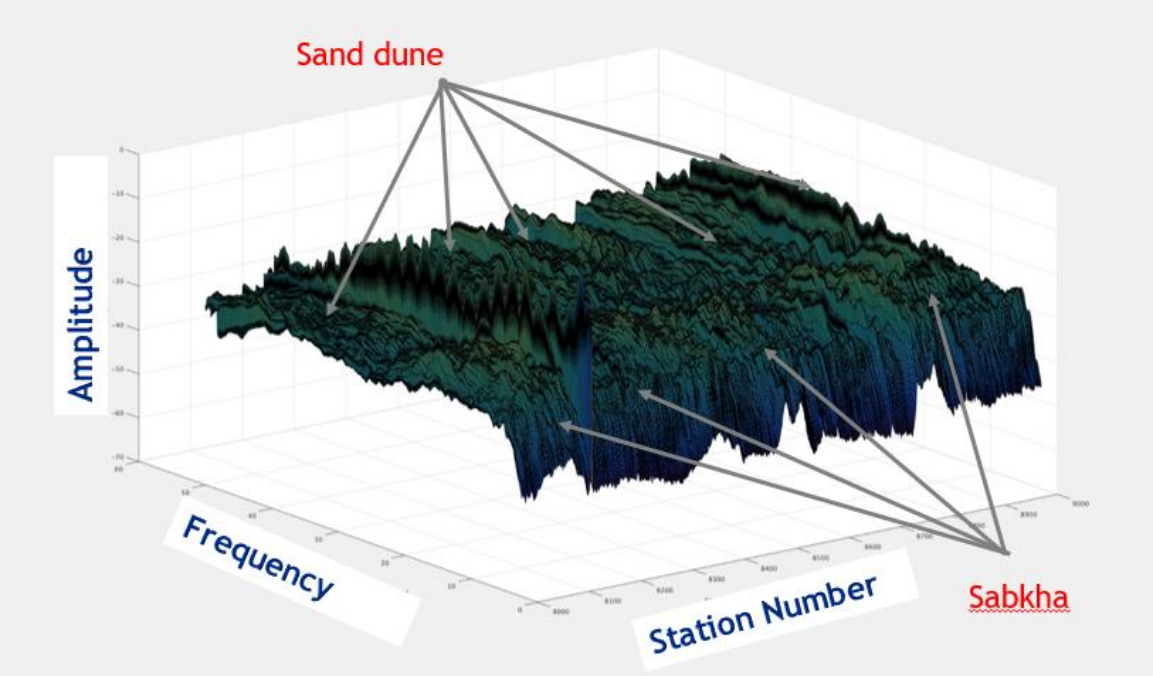

Figure 6.12 the average amplitude spectrum associated with the first 100 stations after the amplitude correction. The graph is displayed with frequency- y-axis, in Hertz, and station number x-axis; the z-axis represents the relative amplitude energy in decibel.

The same dataset was processed using two different workflows to evaluate the effect of the new surface consistent scaling methods on subsequence processes with the aim of obtaining wideband seismic data to improve the suitability of the data for AVO analysis. The raw gathers were processed using a specialized sequences and a conventional sequences; the only difference between the two workflows is the application of the proposed sand dune amplification correction and Gap deconvolution prior to the application of noise attenuation. Figure 6.13 illustrates the two processing flows applied to the seismic data.

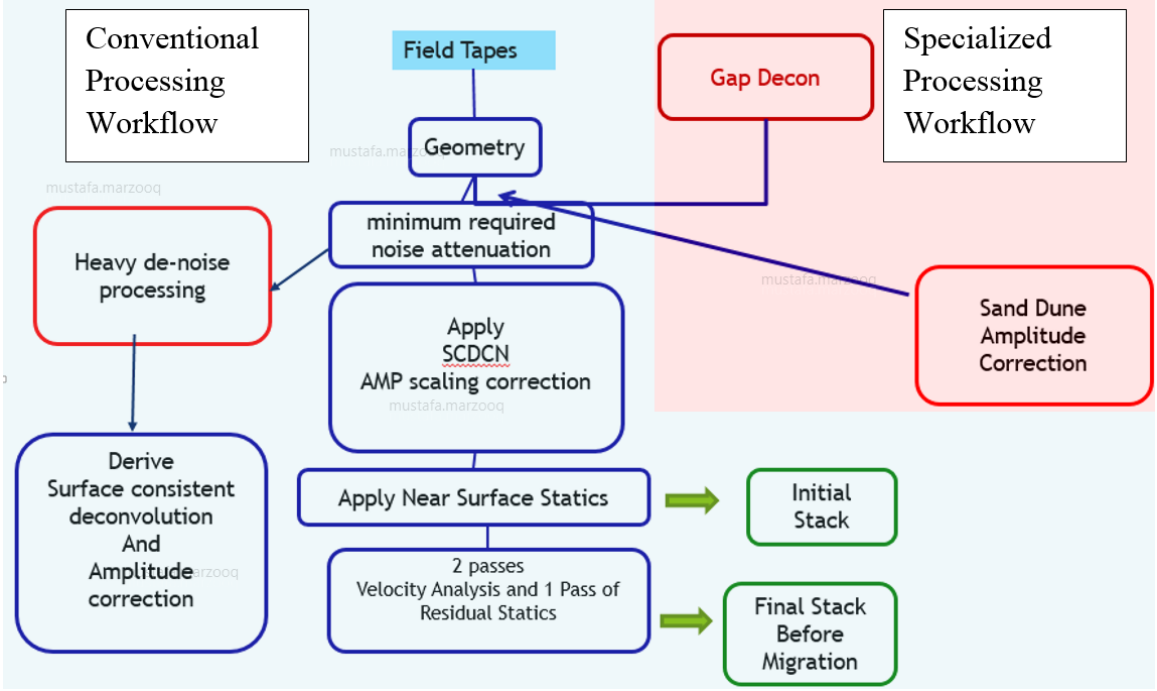

Figure 6.13 Processing flow applied to the real data set.

The raw shot gather shown in Figure 6.14 has a strong ground roll noise that obscures the signal and is characterized by low group velocity and low frequency. Figure 6.15 shows the same shot record as Figure 6.14 with the sand dune amplification correction and gap deconvolution applied. Overall, the specialized workflow reduced the amplification effects in the record. Following the correction, the RMS discrepancy in the offset direction is more consistent with the trend observed on a shot record without the dune on the surface, and I observed a significant improvement in the S/N of traces from the sand dune environment. Importantly, the traces collected in the Sabkha were not altered by the de-amplification step.

In the case of noise attenuation, two noise attenuation techniques based on the F-K transform, T-X to F-K, were applied separately in this project. The F-K filter attempts to

attenuate ground roll noise, given the frequency cut off and the ground roll velocity by creating low-frequency arrays. The filter transforms the gather to the frequency-space domain, where frequency components above than the specified frequency remain unaltered. The frequency-wavenumber (F-K) spectra corresponding to Figure 6.13 and 6.14 demonstrate that, following the sand dune amplification and Gap Deconvolution, the method significantly attenuated scattered energy caused by presence of the dune, allowing the signal and surface wave to be more visible. Consequently, the design of a suitable F-K filter to remove the low frequency surface waves is more convenient with the spatialized workflow. In both workflows, I applied four successive filters to attenuates the noise (200, 500, 600 and 700 m/s) with a frequency cut-off of 15 Hz.

In addition, following the correction, the near surface effects are accounted for and the large discrepancy on the recorded signal (very high amplitude traces) were eliminated from the data being analyzed. With the application of the proposed method, the conventional surface consistent scaling method could resolve the decomposition components without leaking between the different components involved in the decomposition.

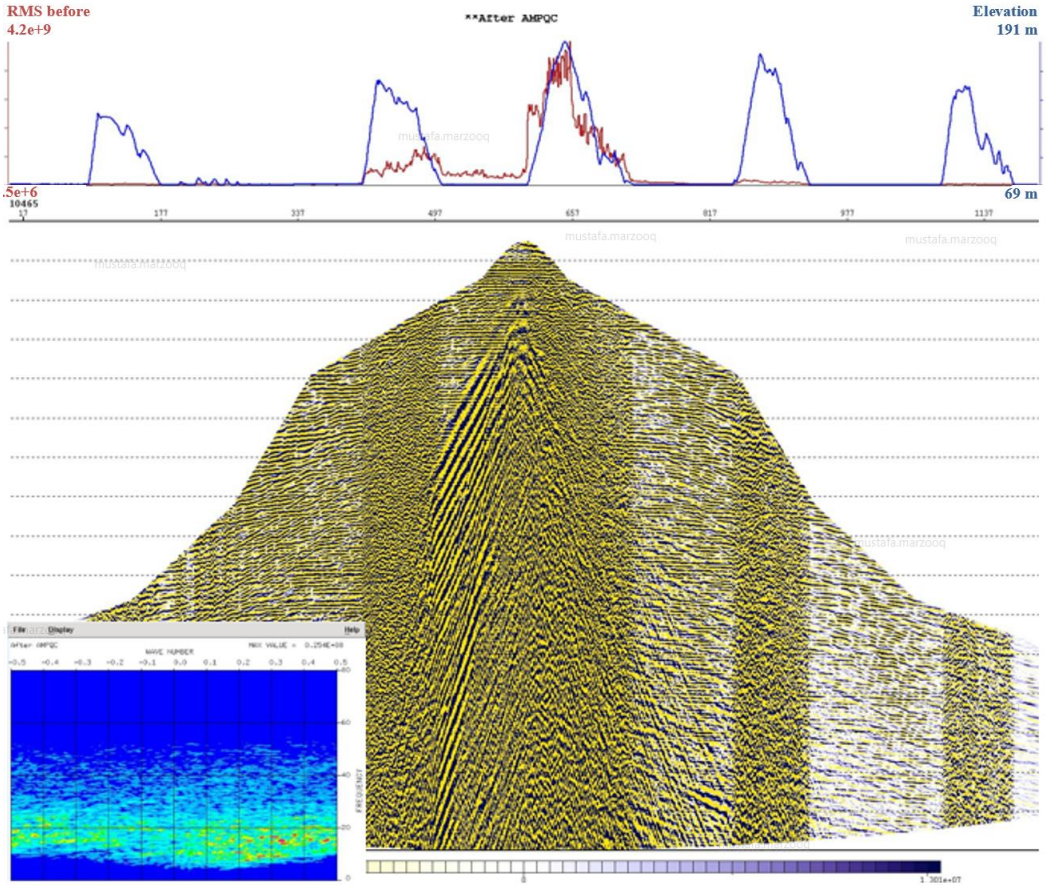

Figure 6.14 A raw field record with geometric spreading correction. The blue and red curves on the top represent sand dune elevation and the RMS amplitude, respectively.

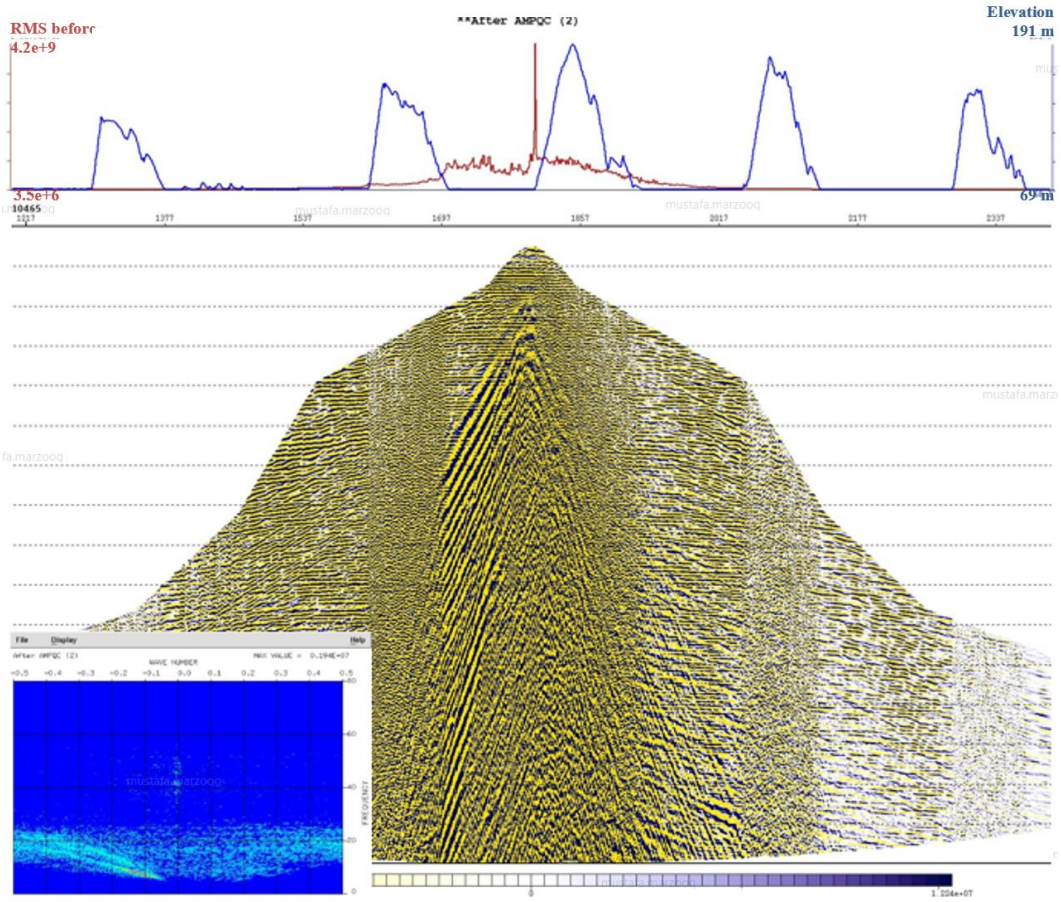

Figure 6.15 The same field record as in Figure 6.14 following the application of the sand dune amplification correction. The blue and red curves on the top represent the sand dune elevation and the RMS amplitude, respectively.

The final stack before migration section for the two workflows are shown in Figure 6.16 and Figure 6.17. The section processed using the conventional workflow shows a spatial amplitude banding on the stack. Overall, the specialized workflow reduced the observed banding effects caused by the dune and the amplitude variation is more consistent with the trend observed on a record without the dune on the surface.

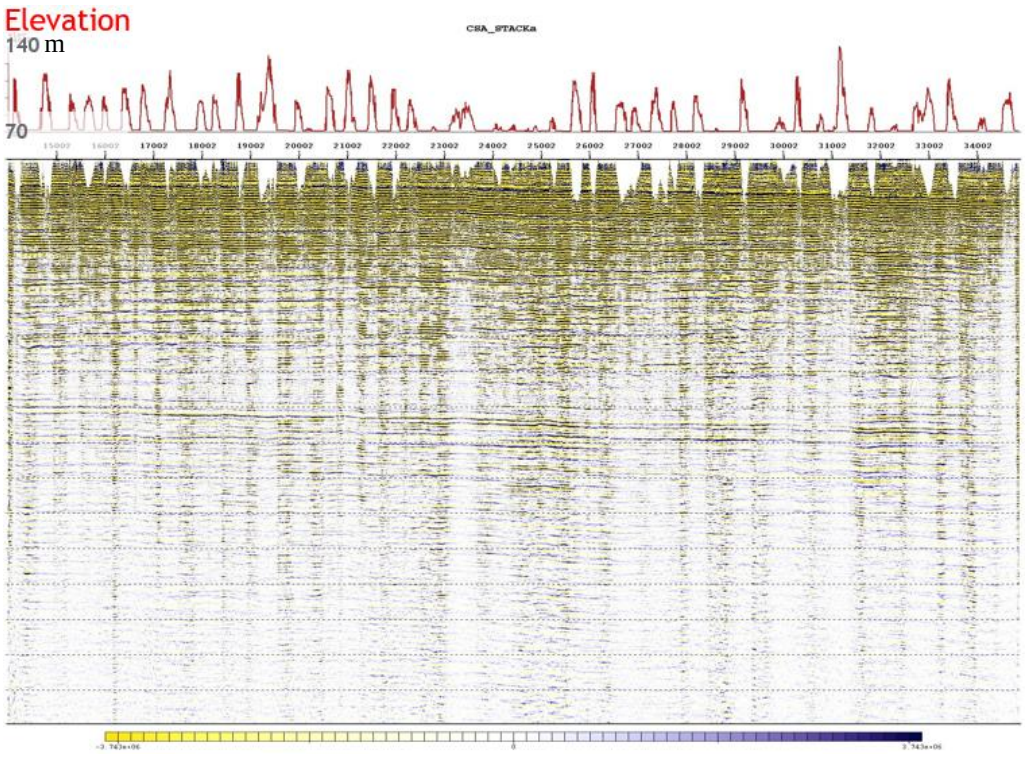

Figure 6.16 A portion of a CMP final stack before migration without the application of the sand dune amplification correction. The red curves on the top represent the sand dune elevation.

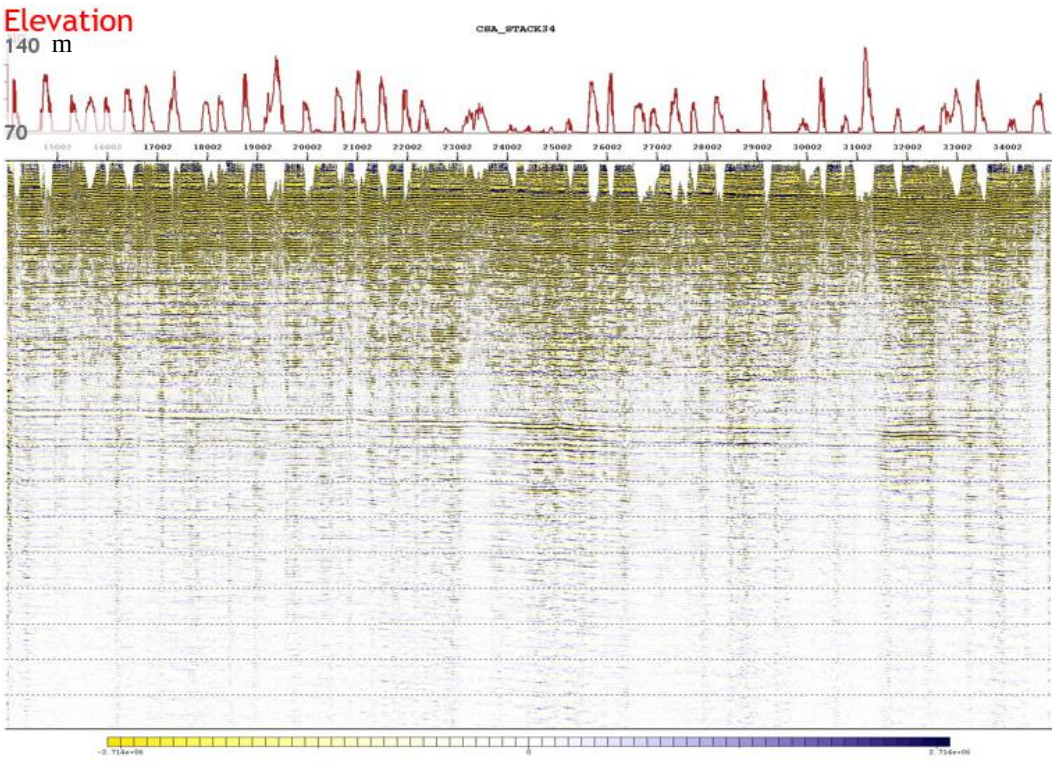

Figure 6.17 A portion of a CMP final stack before migration with the application of the sand dune amplification correction. The red curves on the top represent the sand dune elevation. Note that the observed banding effects caused by the dune were reduced.

CHAPTER 7

CONCLUSIONS AND RECOMMENDATIONS

7.1 Conclusions

The conventional method treats surface-consistent amplitude variation as a frequency-independent and stationary problem. Due to varying near-surface conditions, the surface-consistent amplitude issue is frequency-dependent. In this study, I have proposed a method that can significantly reduce sand-dune amplification effects on seismic data from the Rub Al-Khali desert. The amplification correction factors are frequency dependent and are derived in a surface consistent manner, making the data suitable for further AVO compliant processing steps. The method operates on the dataset at a very early stage of processing. Therefore, only variable gap deconvolution (to attenuate reverberation within the sand dune body) may be needed prior to the application of the method. The method is deterministic in nature; therefore, amplification correction is applied only to stations located on sand dunes. Synthetic data and real data demonstrate that the proposed scaling method can preserve AVO and yield more balanced and consistent amplitude gathers for further noise attenuation. In the case of synthetic examples, I preformed finite difference simulations and tested the sensitivity of the method. I also applied the proposed method to a real data set. The proposed surface-consistent scaling method reduces the relative amplitude variations caused by the

presence of the dune and resulted in seismic data with more balanced amplitudes and higher resolution.

The same dataset was processed using two different workflows to evaluate the effect of the new surface consistent scaling methods on subsequence processes with the aim of obtaining wideband seismic data to improve AVO analyses. The raw gathers were fully processed using two sequences, a specialized one, and a conventional one; the only variation between the two workflows is the application of the proposed dune amplification correction before the application of noise attenuation processes. As expected, the specialized processing flow resulted in a better-balanced section.

7.2 Limitation and Recommendation

The primary goal of this study was to develop and evaluate a new methodology to deal with the sand dunes imprints in the recorded signal. In this section, I discuss some of the limitation of this study.

- The developed methodology does not account for the attenuation. A reliable estimate of seismic attenuation is critical for the realistic assessment of the seismic amplification. Olsen et al. (1995) found that the low-quality factor (Q) values in alluvial sediments have an important influence on ground motions in the sand dunes amplification, and the analysis of reflection coefficients shows that attenuation should be considered in amplitude variation with offset (AVO) studies.
- The sand dunes complex topography changes cannot be handled in the simulation by Finite Difference Method (FDM). Although FDM is a powerful numerical

technique for understanding the types of waves that would be produced by a given Earth structure model, the finite difference method cannot handle complex (e.g., curved domains, fractures) geometries. On the other hand, the finite element is more flexible in modeling complex boundary conditions and complicated geometry. Therefore, any future attempts should consider using Finite Element Method (FEM) which allows the adaptive/local procedure to get higher order local approximation or battling singularities.

- The reference traces should be computed from traces with similar offsets that consistently cover the dune and Sabkha areas. This is not always achievable with actual data in part because of the challenging terrain conditions and the fact that data acquisition is not designed to optimize offset distribution for amplification correction. The method limits the impact of irregular offset distribution, by the flexibility in choosing the offsets range included in the computation of reference traces. Nevertheless, this flexibility is limited when the whole 2D line is covered by a sand dune.

Bibliography

Adan, S., & Rollins, K. (1993). Damage potential index mapping for Salt Lake Valley, Utah,. *Utah Geol. surv*, Pub. 93–4.

Al-Shuhail, A., & Al-Shaibani, A. (2009). Seismic investigation of two coastal Sabkhas, Eastern Saudi Arabia. *Journal of Seismic Exploration*, *18*(4),329–345.

Alterman, Z., & Karal, C. (1968). Propagation of elastic waves in layered media by Finite Difference methods. *Bulletin of the Seismological Society of America.*, *58*, 367–398.

Anderson, J., Bodin, P., Brune, J., Prince, J., Singh, S., Quaas, R., & Onate, M. (1986). Strong ground motion from the Michoacan, Mexico, earthquake. *Science*, *233*, 1043–1049.

Bard, P., & Bouchon, M. (1980). The seismic response of sediment filled valleys, Part 1. The case of incident SH-waves. *Bulletin of Seismological Society of America*, *70*, 1263–1286.

Bard, P. Y., & Bouchon, M. (1985). The two-dimensional resonance of sediment filled valleys. *Bulletin of Seismological Society of America*, *75*, 519-541.

Benz, M. H., & Smith, B. R. (1988). Elastic-wave propagation and site amplification in the Salt Lake valley, Utah, from simulated normal faulting earthquakes. *Bulletin of Seismological Society of America*, *78*, 1851–1874.

Bonilla, L. F., Steidl J. H., Lindley G. T., Tumarkin A. G., & Archuleta R. J. (1997). Site amplification in the San Fernando Valley, California variability of site-effect estimation using the S-wave, coda, and H/V method. *Bull. Seism. Soc. Am. 87*,710-730

Bonilla, L., Steidl, J., Lindley, G., Tumarkin, A., & Archuleta, A. (1997). Site amplification in the San Fernando valley, California: Variability of site effect estimation using S-wave, coda, and H/V methods,. *Bull. Seism. Soc. Am*, *87*, 710–730.

Boore, D. (1970). Finite-difference solutions to the equations of elastic wave propagation, with application to Love waves over dipping interfaces. *M.I.T; Ph.D. thesis*.

Boore, D. (1972). Finite-difference methods for seismic wave propagation in heterogeneous materials, in Methods in computational physics. *New York, Academic Press*, 21–22.

Borcherdt, R. D. (1970). Effects of local geology on ground motion near San Francisco Bay. *Bull. seism. Soc. Am*, *60*(1), 29–61.

Cambois, G., & Stoffa, P. L. (1992). Surface-consistent deconvolution in the log/Fourier domain. *Geophysics*, *57*, 823–840.

Cary, P. W., & Lorentz, G. A. (1992). Four-component surface consistent deconvolution. *Geophysics*, *58*, 383–392.

Cary, P., & Lorentz, G. (1992). Four-component surface consistent deconvolution. *Geophysics*, *58*, 383–392.

Cary, P., & Nagarajappa, N. (2013). Questioning the basics of surface-consistent scaling. *SEG Technical Program Expanded Abstracts*, 3100-3200.

Chopra, S., & Castagna, J. (2014). *AVO.* Society of Exploration Geophysicists. In AVO for managers: Pitfalls and solutions. *CREWES Research Report 12*.

Etienne, V., Tonellot, T., Thierry, P., Berthoumieux, V., & Andreolli, C. (2007). Optimization of the seismic modeling with the time-domain finite-difference method. *SEG Technical Program Expanded Abstracts*, 3536-3540.

Field, E., & Jacob, K. (1995). A comparison and test of various site-response estimation techniques, including three that are not reference-site dependent. *Bull. Seism Soc. Am.*, *85*, 1127–1143.

Frankel, A., Carver, D., & Williams, R. (2002). Nonlinear and linear site response and basin effects in Seattle for the M = 6.8 Nisqually, Washington, earthquake. *Bull. seism. Soc. Am*, *92*(6), 2090–2109.

Frankel, A., Hough, S., Friberg, P., & Busby, R. (1991). Observations of Loma Prieta aftershocks from a dense array in Sunnyvale,. *California,Bull. seism. SOC*, Am. *81*, 1900–1922.

Friedmann, V. (1988). *Near-surface sand effects.* First Break.

Holzer, T. L. (1994). Loma Prieta damage largely attributed to enhanced ground shaking. *EOS Trans. Am. Geophys. Union*, *75*, 299–301.

Kawase, H., & Aki, K. (1989). A study on the response of a soft basin for incident S, P and Rayleigh waves with special reference to the long duration observed in Mexico City. *Bull. seism. SOC,* Am., *79*,1361–1382.

Kelly, K. R., Ward, R. W., Treitel, S., & Alford, R. M. (1976). Synthetic seismograms: A finite -difference approach. *Geophysics*, *41*(1), 2–27.

Kelly, K. R., Ward, R., Treitel, W., & Alford, R. (1976). Synthetic seismograms: A finite-difference approach. *Geophysics*, *41*, 2–27.

Kostadinov, M.v., and Towhata, I. (2002). Assessment of Liquefaction-Inducing Peak Ground Velocity and Frequency of Horizontal Ground Shaking at Onset of Phenomenon." Soil Dynamics and Earthquake Engineering, vol. 22, no. 4, pp. 309–322., doi:10.1016 /s0267-7261(02)00018-0.

Lees, J., & Park, J. (1995). Multiple-taper spectral analysis: A stand-alone C-subroutine. *Computers and Geosciences, 21(2),*199-236.

Levander, A. (1988). Fourth-order finite-difference P-W seismograms. *Geophysics*, *53*(11), 1425–1436.

Levin, S. A. (1989). Surface-consistent deconvolution. *Geophysics*, *54*(9), 1123–1133.

Liner, C. (2008). The seismic sand curve revisited. *Geophysics*, *73*(1), A7–A10.

Loukakis, K. E., & Bielak, J.(1995) Seismic Response of 20-Valleys: Local Site Effects. I*nternational Conferences on Recent Advances in Geotechnical Earthquake Engineering and Soil Dynamics. 11*.

Madariaga, R. (1976). Dynamics of an expanding circular fault: *Bull. Seis. Sot. Am., 66*, 639-666.

Moczo, P., Labak, P., Kristek, & Hron, F. (1996). Amplification and differential motion due to an antiplane 2D resonance in the sediment valleys embedded in a layer over the halfspace. *Bull. Seis. Soc. Am., 85*, 1507–1512.

Mondal, J., & Kumar, A. (2015). Impact of Frequency Content of Input Motion Upon Local Site Effect. *Indian Geotechnical Conference.*

Olsen, K., & Schuster, G. (1995). Causes of low-frequency ground motion amplification in the Salt Lake Basin: The case of the vertically incident P wave. *Geophys. J. Int*, 122, 1045–1061.

Ostrander, W. J. (1984). Plane-wave reflection coefficients for gas sands at non-normal angles of incidence. *Geophysics*, 49(10), 1637–1648.

Parolai, S., Bindi, D., & Augliera, P. (2000). Application of the generalized inversion technique (GIT) to a microzonation study: Numerical simulations and comparison with different site-estimation techniques. *Bull. Seism. Soc. Am.*, *90*, 286–297.

Picozzi, M., Parolai, S., & Albarello, D. (2005). Statistical analysis of noise horizontal-to-vertical spectral ratios (HVSR). *Bull. seism. Soc. Am*, *95*(5), 1779–1786.

Pratt, T., Brocher, T., Weaver, C., Snelson, C., Crosson, R., Miller, K., & Trehu, A. (2003). Amplification of Seismic Waves by the Seattle Basin, Washington State. *Bull. seism. Soc. Am*, *93*(2), 533–545.

Robinson, D. K., & Al-Husseini, M. I. (1982). Technique for reflection prospecting in the Rub' Al-Khali. *Geophysics*, *47*(8), 1135–1152.

Rodgers, A., Patersson, N., & Sjogreen, B. (2010). Simulation of topographic effects on seismic waves from shallow explosions near the North Korean nuclear test site with emphasis on shear wave generation. *Journal of Geoophysical Reserach, 115* (B11).

Rogers, A. M., Borcherdt, R. D., Covington, P. A., & Perkins, M. D. (1984). A comparative ground response study near Los Angeles using recordings of Nevada nuclear tests and the 1971 San Fernando earthquake. *The Seismological Society of America*, *74*(5), 1925–194.

Shan, G. (2009). Optimized implicit finite-difference and Fourier finite-difference migration for VTI media. *Geophysics*, *74*(6), WCA189–WCA197.

Strang, G., & Fix, G. (1973). An analysis of the finite element method. (Series in Automatic Computation). *Journal of Applied Mathematics and Mechanics*, *55*(11), 696–697.

Taner, M. T., & Koehler, F. (1981). Surface consistent corrections. *Geophysics*, *46*, 17–22.

Thomson, J. D. (1982). Spectrum estimation and harmonic analysis. *IEEE Proc.*, *70*, 1077-1096.

Virieux, J. (1986). P-SV wave propagation in heterogeneous media velocity-stress finite-difference method. *Geophysics*, *51*, 889–901.

Vossen, R. V., Curtis, A., Laake, A., & Trampert, J. (2006). Surface-consistent amplitude corrections for single or multicomponent sources and receivers using reciprocity and waveform inversion. *Geophysics*, *71*(2), V19–V30.

Wu, C., Harris, J., Nihei, K., & Nakagawa, S. (2005). Two-dimensional finite-difference seismic modeling of an open fluid-filled fracture: Comparison of thin-layer and linear-slip models. *Geophysics*, *70*(4), T57–T62.

Yu, G., 1985, Offset-amplitude variation and controlled-amplitude processing: *Geophysics*, *50*, 2697–2708.

Vitae

Name	:	Mustafa Al-Marzooq
Nationality	:	Saudi Arabia
Date of Birth	:	4/13/1990
Email	:	marzooq299@gmail.com
Address	:	P.O. Box 11782 Saudi Aramco Dhahran 31311, Saudi Arabia
Academic Background	:	B.S in Geophysics, 2012, University of Tulsa, Tulsa, Oklahoma, United States. M.S. in Geophysics, 2017, King Fahd University of Petroleum and Minerals.
Research Papers	:	Mitigating the Effects of Sand Dunes on Seismic Data from the Rub Al Khali Deserts. Geophysical Prospecting Journal (awaiting reviewer scores-under consideration).